

1 **Interactive comment on ““Measurement report: Statistical modelling of long-term**
2 **atmospheric inorganic gaseous species trends within proximity of the pollution hotspot in**
3 **South Africa” by Jan-Stefan Swartz et al. (Ref. No.: acp-2020-166)**

4 (Reviewers' comments are indicated in black and the response to reviewers are indicated in blue)

5 **Anonymous Referee #1**

6 Received and published: 4 May 2020

7 Overview & Recommendation Sixteen-to nineteen-year records of three important air quality
8 constituents, sulfur dioxide (SO₂), ozone (O₃), nitrogen dioxide (NO₂), that are important over the
9 South African Highveld - ranging from highly populated and industrialized to savanna parkland, are
10 presented for the mid-late 1990s through 2015. The measurements were made at three stations with
11 varying pollution influences, with passive (time-integrated) samplers. The monthly variation and trends
12 in the three trace gases have been identified through a standard multilinear regression model (MLRM).
13 Analysis of the predominant forcings is carried out using terms representing “regional” influences, local
14 meteorology, humidity, proxies for emissions, vs “global” (e.g., ENSO, SAM, IOD, season). A
15 comparison of South African stations with passive sampler results from other locations concludes the
16 paper. The three South African stations represent a contrast of ecosystem and levels of pollution. Levels
17 of certain pollutants are similar to those in polluted Asian areas. Improvements in air quality standards
18 and implementation made progress in reducing emissions around 2000 in the Highveld "pollution hot
19 spot" area, but by 2005 an uptick with more economic development was observed. The results of this
20 study are of great interest, analysis techniques are novel and they are presented with appropriate
21 interpretation. They will be of interest to scientists and policymakers alike. Recommend publication.

22 We would like to thank Referee #1 for the extremely positive review of this paper whereby the relevance
23 of the scientific work is acknowledged, which will be of interest to the broader scientific community
24 and policymakers. We are also very thankful for recommending publication of the paper without any
25 revisions.

26

27

28 **Anonymous Referee #2**

29 Received and published: 12 May 2020

30 South African Highveld area is a heavily industrialized pollution hotspot with a significant regional
31 impact and an area which demonstrates the impacts of growing urban population. There are only limited
32 number of air pollution observations from this kind of areas, and long-term observations are even more
33 scarce.

34 The limitation of the method (observations) applied in this paper is the monthly time resolution, which
35 prevents the use of the method on e.g. AQ observations required by the legislation. In addition, due to
36 the regional circulation pattern, the applied measurement sites are often upwind of the most polluted
37 region, so they do not necessarily represent the highest regional concentrations in the Highveld area,
38 which is also clear when Figures A4 and A5 are compared with the maps in Figs 1 and 2.

39 As the manuscript is well-written and provides a rare data set with regional / global scientific
40 importance, I recommend the publication of the manuscript, after the following minor issues are
41 addressed.

42 We would like to thank Referee #2 for the very positive review of this paper and recommending
43 publication of the manuscript, through realising the value of this long-term atmospheric gaseous dataset
44 for this regionally and globally important region. We would also like to thank Referee #2 for the minor
45 suggestions made, which were each carefully considered and addressed/implemented in the paper.
46 Below is a point-by-point response to each of these comments/questions. In addition, a marked-up
47 version of the revised manuscript is also provided indicating all changes made throughout the
48 manuscript.

49

50 1) Abstract: please provide some numeric values for average monthly SO₂, NO₂ and O₃-concentrations
51 observed.

52 We thank Referee #2 for this suggestion. We have included the average monthly SO₂, NO₂ and O₃
53 concentrations at the three sites in the Abstract as requested as follows:

54 "...north-eastern interior in South Africa. The interdependencies between local, regional and global
55 parameters on variances in SO₂, NO₂ and O₃ levels were investigated in the model. Average monthly
56 SO₂ concentrations at Amersfoort (AF), Louis Trichardt (LT) and Skukuza (SK) were 9.91 µg/m³, 1.70
57 µg/m³ and 2.07 µg/m³, respectively, while respective mean monthly NO₂ concentrations at each of these
58 sites were 6.56 µg/m³, 1.46 µg/m³ and 2.54 µg/m³. Average monthly O₃ concentrations were 50.77

59 $\mu\text{g}/\text{m}^3$, 58.44 $\mu\text{g}/\text{m}^3$ and 43.36 $\mu\text{g}/\text{m}^3$ at AF, LT and SK, respectively. Long-term temporal trends
60 indicated seasonal and inter-annual variability at all three sites, which could be ascribed to...”

61

62 2) One of the basic principles in ACP is the open-access data following FAIR principles. Please include
63 the obligatory “Data availability” paragraph and provide the data, with necessary metadata, shown in
64 Figures A1, A2 and A3. Extracting the data from these figures is in any case very straightforward
65 process, so having it directly in numeric format will save some time for co-scientists using the dataset
66 e.g. as ground-truth for remote sensing observations, or reference data for global models. If the data are
67 not provided, please give a proper justification.

68 We agree with the open-access data policy and FAIR principles followed by ACP. However, these
69 datasets were collected in the INDAAF (International Network to study Deposition and Atmospheric
70 composition in Africa) network, which is part of the DEBITS (Deposition of Biogeochemical Important
71 Trace Species) project endorsed by the International and Global Chemistry (IGAC) programme ([www.
72 https://indaaf.obs-mip.fr/](http://www.https://indaaf.obs-mip.fr/)). It is indicated on the INDAAF website that data will be made available upon
73 request, since there are data sharing policies that entail co-authorship on papers utilising data collected
74 within this network. Therefore, data is made available upon request and agreement with our data sharing
75 policies. Furthermore, these datasets are also currently utilised in other papers being currently prepared.
76 We have included the obligatory “Data availability” section in the paper as follows:

77 **“5. Data availability**

78 The data of this paper are available upon request to Pieter van Zyl (pieter.vanzyl@nwu.ac.za) or Paul
79 Beukes (paul.beukes@nwu.ac.za).”

80

81 3) Please indicate AF, LT and SK sites in the figures A4 and A5, as this comparison provides
82 information on regional significance of the observations (i.e. what are the concentrations at these sites
83 compared to areas with highest concentrations in the area).

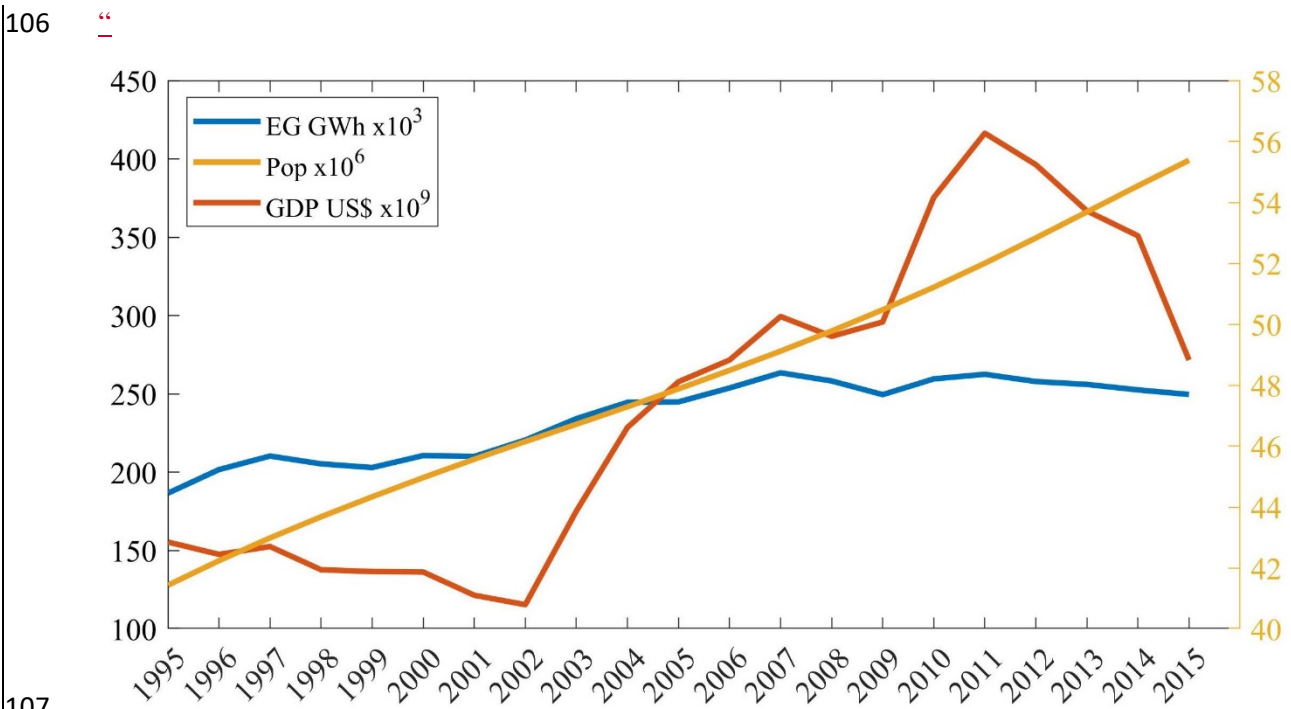
84 We completely agree with Referee #2 that inclusion of AF, LT and SK in these figures would assist in
85 contextualising these sites within this region. However, these figures were extracted from the NASA
86 Giovanni satellite data on the NASA website (as indicated in the figure captions) and we are therefore
87 not able to make any changes on these figures. It might be possible to conduct edits manually by using
88 imaging software, but the sites will not be accurately located on the map (exact coordinates) and it could
89 also possibly decrease the quality of these maps. In addition, these maps are only included as supportive
90 material in the Appendix to contextualise the location of the three sites as discussed in **Section 3.3**

91 **Contextualisation.** We are of the opinion that relating Figure 1 to these two figures does assist the
92 reader do contextualise the location of these sites to the satellite date presented for this region in these
93 two figures.

94

95 4) In several parts of the manuscript, results/trends are explained to be due to the changes in economy
96 and/or population. Annual data on GDP, population and energy production is easily available on IEA
97 and World Bank www-pages (and potentially also from Statistics South Africa). To support the
98 explanations in the manuscript, please include a figure showing these three societal variables for the
99 period 1995-2015, and refer to this figure in the text.

100 We thank Referee #2 for this comment and completely agree that GDP, population and energy
101 production data would support the observed trends. A figure was compiled including the South African
102 population and GDP as obtained from the World Bank website
103 (<https://data.worldbank.org/country/south-africa>), while electricity production data was acquired from
104 the International Energy Agency ([https://www.iea.org/data-and-statistics/data-](https://www.iea.org/data-and-statistics/data-tables?country=SOUTHAFRIC)
105 [tables?country=SOUTHAFRIC](https://www.iea.org/data-and-statistics/data-tables?country=SOUTHAFRIC)). This figure (Fig. A4) was included in the Appendix:



108 **Figure A4:** South African population (Pop) and GDP from 1995 to 2015 (World Bank, 2019), as
109 well as electricity generation (EG) during this period (International Energy Agency, 2020)”

110 The following sentences were added in the third paragraph of Section 3.2.1 Sulphur dioxide (SO₂),
111 which refers to this new figure:

112 “...activities, e.g. increased production by pyrometallurgical industries (ICDA, 2012), as well as the
113 increase in population growth accompanied by higher energy demand (Vet et al., 2014). In Fig. A4, the
114 South African population and GDP from 1995 to 2015 according to the World Bank (World Bank,
115 2019) are presented together with the electricity generation (EG) in South Africa during this period as
116 indicated by the International Energy Agency (International Energy Agency, 2020). A continuous
117 growth in population is observed from 1995 to 2015, while the GDP trend reflects economic growth
118 during this period corresponding to the observed periods of decreased and increased SO₂ concentrations.
119 A general increase in electricity production over this period is also evident. Electricity consumption is
120 a good indicator of increased anthropogenic activities, with Inglesi-Lotz and Blignaut (2011)
121 indicating...”

122 The following references were also added to the Reference list:

123 “International Energy Agency. 2020. Data and statistics [Online]. Available: [https://www.iea.org/data-](https://www.iea.org/data-and-statistics/data-tables?country=SOUTHAFRIC)
124 [and-statistics/data-tables?country=SOUTHAFRIC](https://www.iea.org/data-and-statistics/data-tables?country=SOUTHAFRIC) [Accessed 14 May 2020]”

125 “World Bank. 2019. Data [Online]. Available: <https://data.worldbank.org/country/south-africa>
126 [Accessed 15 May 2020].”

127 These two references were also cited in the first paragraph of the Introduction as follows:

128 “...generation (Rorich and Galpin, 1998; Tiitta et al., 2014). Atmospheric pollution associated with
129 South Africa is compounded by high population growth that, in turn, drives further economic and
130 industrial growth leading to an ever-increasing energy demand (Tiitta et al., 2014; World Bank, 2019;
131 International Energy Agency, 2020). The extent of air pollution...”

132

133 5) For clarity, if possible, please change color axes in Figs A4 and A5 to include less decimals

134 As indicated in our response to Comment 3 of Referee #2, these figures were extracted from the NASA
135 Giovanni satellite data on the NASA website (as indicated in the figure captions) and we are therefore
136 not able to make any changes on these figures, which include changes to decimals and colour axes.

137

138

Measurement report: Statistical modelling of long-term atmospheric inorganic gaseous species trends within proximity of the pollution hotspot in South Africa

Jan-Stefan Swartz¹, Pieter G. Van Zyl^{1*}, Johan P. Beukes¹, Corinne Galy-Lacaux², Avishkar Ramandh³, Jacobus J. Pienaar¹

¹ Atmospheric Chemistry Research Group, Chemical Resource Beneficiation, North-West University, Potchefstroom Campus, Potchefstroom, 2520, South Africa

² Laboratoire d'Aerologie, UMR 5560, Université Paul-Sabatier (UPS) and CNRS, Toulouse, France

³ Sasol Technology R&D (Pty) Limited, Sasolburg, South Africa

*Corresponding author: P.G. van Zyl (pieter.vanzyl@nwu.ac.za)

Abstract

South Africa is considered an important source region of atmospheric pollutants, which is compounded by high population- and industrial growth. However, this region is understudied, especially with regard to evaluating long-term trends of atmospheric pollutants. The aim of this study was to perform statistical modelling of SO₂, NO₂ and O₃ long-term trends based on 21-, 19- and 16-year passive sampling datasets available for three South African INDAAF (International network to study Atmospheric Chemistry and Deposition in Africa) sites located within proximity of the pollution hotspot in the industrialised north-eastern interior in South Africa. The interdependencies between local, regional and global parameters on variances in SO₂, NO₂ and O₃ levels were investigated in the model. [Average monthly SO₂ concentrations at Amersfoort \(AF\), Louis Trichardt \(LT\) and Skukuza \(SK\) were 9.91 µg/m³, 1.70 µg/m³ and 2.07 µg/m³, respectively, while respective mean monthly NO₂ concentrations at each of these sites were 6.56 µg/m³, 1.46 µg/m³ and 2.54 µg/m³. Average monthly O₃ concentrations were 50.77 µg/m³, 58.44 µg/m³ and 43.36 µg/m³ at AF, LT and SK, respectively.](#) Long-term temporal trends indicated seasonal and inter-annual variability at all three sites, which could be ascribed to changes in meteorological conditions and/or variances in source contribution. Local, regional and global parameters contributed to SO₂ variability, with total solar irradiation (TSI) being the most significant factor at the regional background site, [Louis Trichardt \(LT\)](#). Temperature (T) was the most important factor at [Skukuza \(SK\)](#), located in the Kruger National Park, while population growth (P) made the most substantial contribution at the industrially impacted [Amersfoort \(AF\)](#) site. Air masses passing over the source region also contributed to

171 SO₂ levels at SK and LT. Local and regional factors made more substantial contributions to
172 modelled NO₂ levels, with P being the most significant factor explaining NO₂ variability at all
173 three sites, while relative humidity (RH) was the most important local and regional
174 meteorological factor. The important contribution of P on modelled SO₂ and NO₂
175 concentrations was indicative of the impact of increased anthropogenic activities and energy
176 demand in the north-eastern interior of South Africa. Higher SO₂ concentrations, associated
177 with lower temperatures, as well as the negative correlation of NO₂ levels to RH, reflected the
178 influence of pollution build-up and increased household combustion during winter. El-Niño
179 Southern Oscillation (ENSO) made a significant contribution to modelled O₃ levels at all three
180 sites, while the influence of local and regional meteorological factors was also evident. Trend
181 lines for SO₂ and NO₂ at AF indicated an increase in SO₂ and NO₂ concentrations over the 19-
182 year sampling period, while an upward trend in NO₂ levels at SK signified the influence of
183 growing rural communities. Marginal trends were observed for SO₂ at SK, as well as SO₂ and
184 NO₂ at LT, while O₃ remained relatively constant at all three sites. SO₂ and NO₂ concentrations
185 were higher at AF, while the regional O₃ problem was evident at all three sites.

186 **Keywords:** passive sampling; sulphur dioxide; nitrogen dioxide; ozone; DEBITS; multiple-
187 linear regression

188

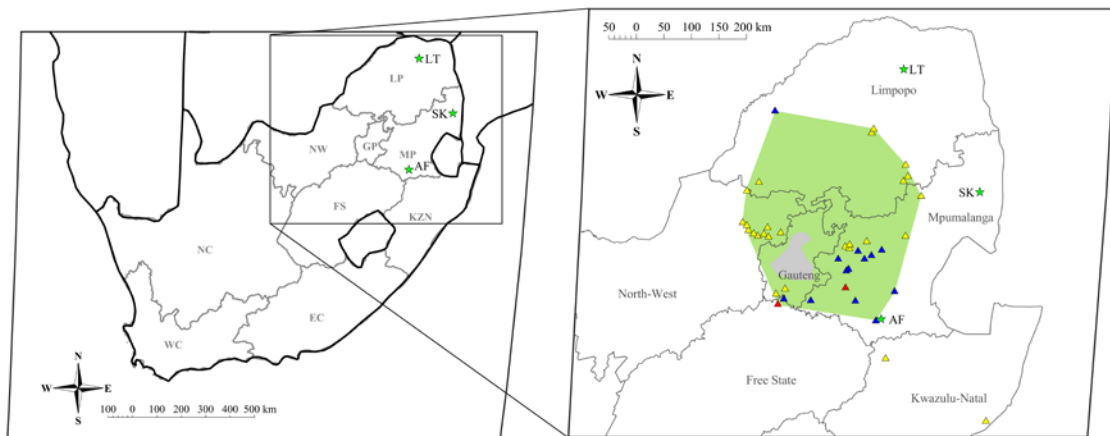
189 1. Introduction

190 Although Africa is regarded as one of the most sensitive continents with regard to air pollution
191 and climate change, it is the least studied (Laakso et al., 2012). South Africa is considered an
192 important source region of atmospheric pollutants within the African continent, which is
193 attributed to its highly industrialised economy with the most significant industrial activities
194 including mining-, metallurgical- and petrochemical activities, as well as large-scale coal-fired
195 electricity generation (Rorich and Galpin, 1998; Tiitta et al., 2014). Atmospheric pollution
196 associated with South Africa is compounded by high population growth that, in turn, drives
197 further economic and industrial growth leading to an ever-increasing energy demand (Tiitta et
198 al., 2014; [World Bank, 2019](#); [International Energy Agency, 2020](#)). The extent of air pollution
199 in South Africa is illustrated by the well-known NO₂ pollution hotspot revealed by satellite
200 data over the Mpumalanga Highveld, where 11 coal-fired power stations are located (Lourens
201 et al., 2011), which was also recently indicated by the newly launched European Space Agency
202 Sentinel 5P satellite (Meth, 2018).

203 The importance of long-term atmospheric chemical measurements has been indicated by
204 numerous studies on atmosphere-biosphere interactions (Fowler et al., 2009) and air quality
205 (Monks et al., 2009). These long-term assessments are crucial in identifying relevant policy
206 requirements on local and global scales, as well as the most topical atmospheric chemistry
207 research questions (Vet et al., 2014; IPCC, 2014). In 1990, the International Global
208 Atmospheric Chemistry (IGAC) programme, in collaboration with the Global Atmosphere
209 Watch (GAW) network of the World Meteorological Organisation (WMO) initiated the
210 Deposition of Biogeochemically Important Trace Species (DEBITS) project with the aim to
211 conduct long-term assessments of atmospheric biogeochemical species in the tropics – a region
212 for which limited data existed (Lacaux et al., 2003). The programme is currently operated
213 within the framework of the third phase of IGAC and within the context of the International
214 Nitrogen Initiative (INI) programme. The African component of this initiative was historically
215 referred to as IGAC DEBITS Africa (IDAF), which was relabelled in 2015/2016 under the
216 International Network to study Atmospheric Chemistry and Deposition in Africa (INDAAF)
217 programme. The INDAAF long-term network currently consists of 13 monitoring sites,
218 strategically positioned in southern-, western- and central Africa, which are representative of
219 the most important African ecosystems (<http://indaaf.obs-mip.fr>). Typical measurements at the
220 INDAAF sites include wet-only rain collection, aerosol composition and inorganic gaseous
221 concentrations, determined with passive samplers.

222 Long-term measurements have been conducted at three dry-savannah southern African
 223 INDAAF sites, which include Amersfoort (AF), Louis Trichardt (LT) and Skukuza (SK)
 224 located within proximity of the pollution hotspot in the north-eastern interior of South Africa.
 225 Measurement of inorganic gaseous pollutant species i.e. sulphur dioxide (SO₂), nitrogen
 226 dioxide (NO₂) and ozone (O₃), have been conducted since 1995 at LT, 1997 at AF and 2000 at
 227 SK utilising passive samplers. These gaseous species are generally associated with the above-
 228 mentioned major sources of atmospheric pollutants in South Africa (Connell, 2005). Moreover,
 229 a large number of these sources are located within the north-eastern interior of South Africa,
 230 and include the Mpumalanga Highveld, the Johannesburg-Pretoria conurbation and the Vaal
 231 Triangle. Laban et al. (2018), for instance, recently indicated high O₃ levels in this north-
 232 eastern interior of South Africa, while it was also indicated that O₃ formation in this region can
 233 be considered NO_x-limited due to high NO₂ concentrations. Therefore, the South African
 234 INDAAF sites were strategically positioned to be representative of the South African interior,
 235 with AF an industrially influenced site, LT a rural background site and SK a background site
 236 located in the Kruger National Park, as indicated in Fig. 1.

237



238 **Figure 1:** Regional map of South Africa indicating the measurement sites at Amersfoort
 239 (AF), Louis Trichardt (LT) and Skukuza (SK) with green stars. A zoomed-in map
 240 indicates the defined source region, the Johannesburg-Pretoria Megacity (grey
 241 polygon) and large point sources, i.e. power stations (blue triangles),
 242 petrochemical plants (red triangles) and pyrometallurgical smelters (yellow
 243 triangles)

244

245 A number of studies have been reported on measurements conducted within the INDAAF
 246 network (Martins et al., 2007; Adon et al., 2010; Josipovic et al., 2011; Adon et al., 2013),

247 presenting inorganic gaseous concentrations at southern-, as well as western- and central
248 African sites, respectively. Conradie et al. (2016) recently reported on precipitation chemistry
249 at the South African INDAAF sites, while Maritz et al. (2020) conducted an assessment of
250 particulate organic- and elemental carbon at these sites. However, in-depth analysis of long-
251 term trends of atmospheric pollutants at the INDAAF sites has not been conducted due to the
252 non-availability of long-term data. Therefore, the aim of this study was to perform statistical
253 modelling of SO₂, NO₂ and O₃ long-term trends based on 21-, 19- and 16-year datasets
254 available for LT, AF and SK, respectively. The influences of sources together with local,
255 regional and global meteorological patterns on the atmospheric concentrations of SO₂, NO₂
256 and O₃ were considered in the model.

257

258 **2 Measurement site and experimental methods**

259 **2.1 Site description**

260 Detailed site descriptions have been presented in literature, e.g. Mphepya et al. (2004),
261 Mphepya et al. (2006) and Conradie et al. (2016). AF (1 628 m amsl) and LT (1 300 m amsl)
262 are located within the South African Highveld, while SK is situated in the South African
263 Lowveld. As indicated in Fig.1, AF is in close proximity to the major industrial activities in
264 the Mpumalanga Highveld (~50 to 100 km north-west) and ~200 km east of the Johannesburg-
265 Pretoria conurbation. LT is located in a rural region mainly associated with agricultural activity,
266 while SK (267 m amsl) is situated in the Kruger National Park, i.e. natural bushveld in a
267 protected area.

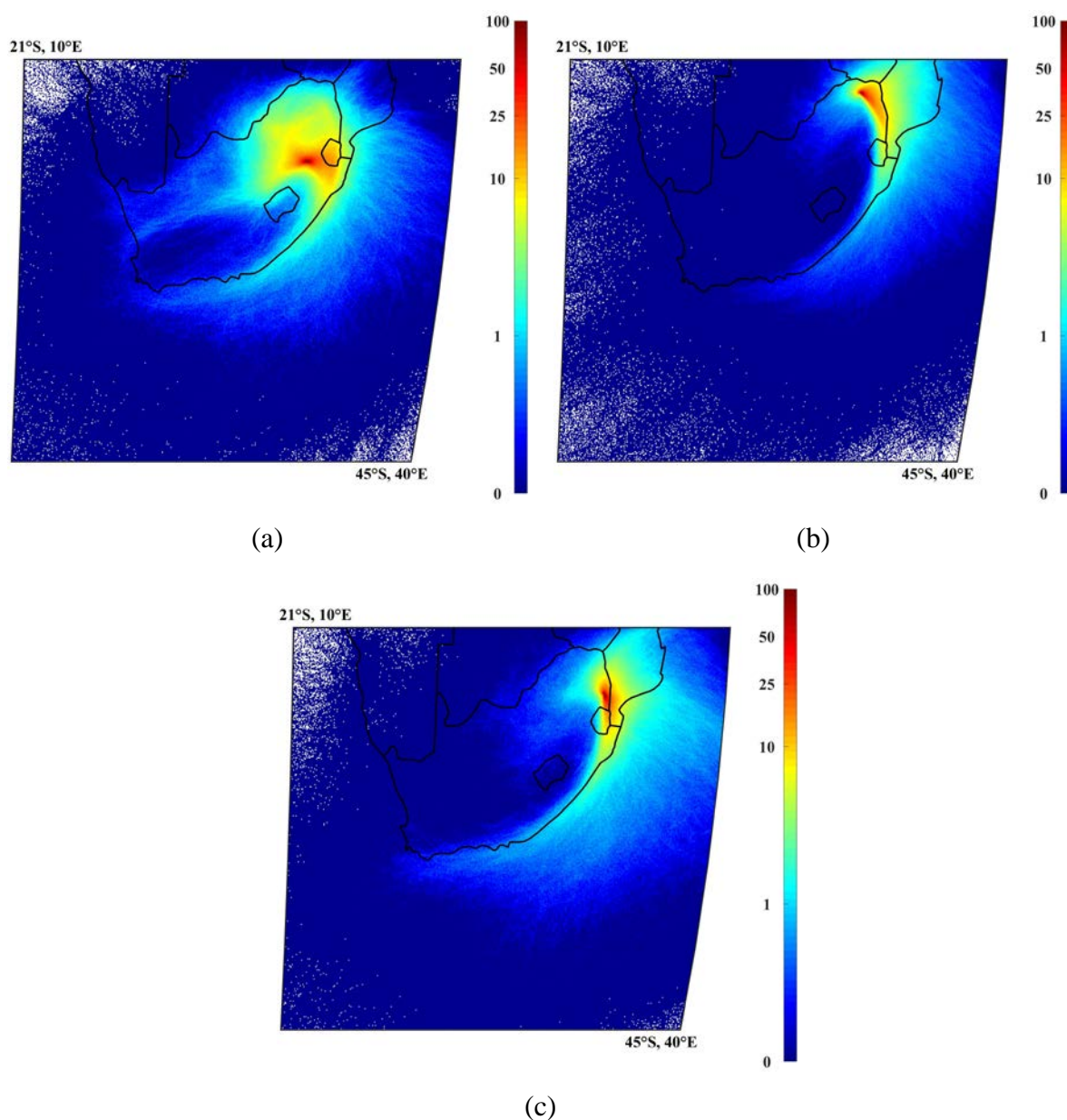
268 A summary of the regional meteorology of the South African interior, especially relating to the
269 north-eastern part, was presented by Laakso et al. (2012) and Conradie et al. (2016).
270 Meteorology in the South African interior exhibits strong seasonal variability. This region is
271 characterised by anticyclonic air mass circulation, which is especially predominant during
272 winter, resulting in pronounced inversion layers trapping pollutants near the surface (Tyson et
273 al., 1996; Garstang et al., 1996; Gierens et al., 2019). In addition, the north-eastern interior (as
274 most parts of the South African interior) is also characterised by distinct wet and dry seasons,
275 with the wet season occurring typically from mid-spring up to autumn (mid-October to mid-
276 May) (Hewitson and Crane, 2006; Conradie et al., 2016).

277 In Fig. 2, the air mass history for LT, AF and SK for the entire sampling periods at each site is
278 presented by means of overlaid back trajectories. 96-hour back trajectories arriving hourly at

279 each site at a height of 100 m were calculated with the Hybrid Single-Particle Lagrangian
280 Integrated Trajectory (HYSPLIT) model (version 4.8), developed by the National Oceanic and
281 Atmospheric Administration (NOAA) Air Resources Laboratory (ARL) (Draxler and Hess,
282 2014).

283 Meteorological data was obtained from the GDAS archive of the National Centre for
284 Environmental Prediction (NCEP) of the United States National Weather Service. Back
285 trajectories were overlaid with fit-for-purpose programming software on a map area divided
286 into grid cells of $0.2^\circ \times 0.2^\circ$. A colour scale presents the frequency of back trajectories passing
287 over each grid cell, with dark blue indicating the lowest and dark red the highest percentage.
288 The predominant anticyclonic air mass circulation over the interior of South Africa is reflected
289 by the overlay back trajectories at each site, while it also indicates that AF is frequently
290 impacted by air masses passing over the major sources in the north-eastern interior. In addition,
291 it is also evident that the rural background sites (LT and SK) are also impacted by the regional
292 circulation of air masses passing over the major sources.

293



294 **Figure 2:** Overlaid hourly arriving 96-hour back-trajectories for air masses arriving at (a)
 295 AF from 1997 to 2015, (b) LT from 1995 to 2015 and (c) SK from 2000-2015

296

297 2.2 Sampling, analysis and data quality

298 Passively derived SO₂, NO₂ and O₃ concentrations were available from 1995 to 2015, 1997 to
 299 2015 and 2000 to 2015 for LT, AF and SK, respectively. Gaseous SO₂, NO₂ and O₃
 300 concentrations were measured utilising passive samplers manufactured at the North-West
 301 University, which are based on the Ferm (1991) passive sampler. Detailed descriptions on the
 302 theory and functioning of these passive samplers, which are based on laminar diffusion and
 303 chemical reaction of the atmospheric pollutant of interest, have been presented in literature

304 (Ferm, 1991; Dhammapala, 1996; Martins et al., 2007; Adon et al., 2010). In addition, the
305 passive samplers utilised in this study have been substantiated through a number of inter-
306 comparison studies (Martins et al., 2007; He and Bala, 2008).

307 Samplers were exposed in duplicate sets for each gaseous species at each measurement site
308 (1.5 m above ground level) for a period of approximately one month and returned to the
309 laboratory for analysis. Blank samples were kept sealed in the containers for each set of
310 exposed samplers. Prior to 2008, SO₂ and O₃ passive samples were analysed with a Dionex
311 100 Ion Chromatograph (IC), while NO₂ samples were analysed with a Cary 50 uv/vis
312 spectrometer up until 2012. SO₂ and O₃ samples collected after 2008, and NO₂ samples
313 collected after 2012, were analysed with a Dionex ICS-3000 system. Data quality of the
314 analytical facilities is ensured through participation in the World Meteorological Organisation
315 (WMO) bi-annual Laboratory Inter-Comparison Study (LIS). The results of the 50th LIS study
316 in 2014 indicated that the recovery of each ion in standard samples was between 95 and 105%
317 (Conradie et al., 2016). Analysed data was also subjected to the Q-test, with a 95% confidence
318 threshold to identify, evaluate and reject outliers in the datasets.

319

320 **2.3 Multiple linear regression model**

321 Similar to the approach employed by Swartz et al. (2020) for the Cape Point GAW station, a
322 multiple linear regression (MLR) model was utilised to statistically evaluate the influence of
323 sources and meteorology on the concentrations of SO₂, NO₂ and O₃ at AF, LT and SK. This
324 model was also utilised by Tohir et al. (2018) and Bencherif et al. (2006) for trend estimates
325 of O₃ and temperature, respectively. MLR analysis models the relationship between two or
326 more independent variables and a dependant variable by fitting a linear equation to the
327 observed data, which can be utilised to calculate values for the dependent variable. In this
328 study, concentrations of inorganic gaseous species (SO₂, NO₂ and O₃) were considered the
329 dependent variable (C(t)), while local, regional and global factors were considered independent
330 variables to yield the following general equation:

$$331 \quad C(t) = \sum_{k=1}^p a(k) \times f(t,k) + R'(t) \quad 1$$

332 where f(t,k) describes the specific factor k at time t; a(k) is the coefficient calculated by the
333 model for the factor k that minimises the root mean square error (RMSE); and R'(t) is the

334 residual term that accounts for factors that may have an influence on the model, which are not
335 considered in the MLR model. The RMSE compares the calculated values with the measured
336 values as follows;

$$337 \quad \chi^2 = [\sum_t C(t) - \sum_k a(k) \times f(t,k)]^2 \quad 2$$

338 The trend was parameterised as linear: Trend (t) = $\alpha_0 + \alpha_1.t$, where t denotes the time range, α_0
339 is a constant, α_1 is the slope of Trend(t) line that estimates the trend over the time scale.

340 The significance of each of the independent variables on the calculated C(t) was evaluated by
341 the relative importance weights (RIW) approach, which examines the relative contribution that
342 each independent variable makes to the dependent variable and ranks independent variables in
343 order of significance (Nathans et al., 2012; Kleynhans et al., 2017). The RIW approach was
344 applied with IBM® SPSS® Statistics Version 23, together with program syntaxes and scripts
345 adapted from Kraha et al. (2012) and Lorenzo-Seva et al. (2010).

346

347 **2.4 Input data**

348 Global meteorological factors considered in the model included Total Solar Irradiation (TSI),
349 the El-Niño Southern Oscillation (ENSO), the Indian Ocean Dipole (IOD), the Quasi-Biennial
350 Oscillation (QBO) and the Southern Annular Mode (SAM). Data for the ENSO and QBO
351 cycles was obtained from the National Oceanic and Atmospheric Administration (NOAA)
352 (NOAA, 2015a; NOAA, 2015b), while TSI and IOD data was obtained from the Royal
353 Netherlands Meteorological Institute (“*Koninklijk Nederlands Meteorologisch Instituut*”)
354 (KMNI, 2016a; KMNI, 2016b). SAM data was obtained from the National Environmental
355 Research Council’s British Antarctic Survey (Marshall, 2018). The initial input parameters for
356 the model only included the global force factors in order to assess the importance of individual
357 global predictors on measured gaseous concentrations.

358 Local and regional meteorological parameters included in the model were rain depth (RF),
359 relative humidity (RH) and ambient temperature (T), as well as monthly averaged wind
360 direction (Wd) and -speed (Ws). Since meteorological parameters were not measured at the
361 three sites during the entire sampling period, meteorological data was obtained from the
362 European Centre for Medium-Range Weather Forecasts (ECMWF) reanalysis-interim archive
363 (ERA). Although meteorological measurements were conducted by the South African Weather
364 Service within relative proximity of the locations of the three sites, the data coverage for all

365 the meteorological parameters for the entire sampling period was relatively low (<50%).
366 Planetary boundary layer (PBL) heights were obtained from the global weather forecast model
367 operated by the ECMWF (Korhonen et al., 2014). Population data (P) from three separate
368 national censuses was obtained from local municipalities and was also included in the model.

369 Daily fire distribution data from 2000 to 2015 was derived from the National Aeronautics and
370 Space Administration's (NASA) Moderate Resolution Imaging Spectrometer (MODIS)
371 satellite retrievals. MODIS is mounted on the polar-orbiting Earth Observation System's (EOS)
372 Terra spacecraft and globally measures, among others, burn scars, fire and smoke distributions.
373 This dataset was retrieved from the NASA Distributed Active Archive Centres (DAAC)
374 (Kaufman et al., 2003). Fire events were separated into local fire events (LFE), occurring
375 within a 100 km radius from a respective site, and regional fire events (DFE), taking place
376 between 100 km and 1 000 km from each site.

377 Hourly arriving back trajectories (as discussed above) were also used to calculate the
378 percentage time that air masses spent over a predefined source region (Fig. 1) before arriving
379 at each of the sites for each month, which was also a parameter (SR) included in the statistical
380 model. The source region is a combination of source regions defined in previous studies, e.g.
381 Jaars et al. (2014) and Booyens et al. (2019), which comprised the Mpumalanga Highveld,
382 Vaal Triangle, the Johannesburg-Pretoria conurbation, the western- and the eastern Bushveld
383 Igneous Complex (Fig. 1).

384 Since data was not available for certain local and regional factors considered in the model for
385 the entire sampling periods at AF, LT and SK, and, in an effort to include the optimum number
386 of local and regional factors available for each site, modelled concentrations could not be
387 calculated for the entire sampling periods when global, regional and local factors were included
388 in the MLR model.

389

390 **3 Results**

391 Fig. A1, A2 and A3 present the time series of monthly average SO₂, NO₂ and O₃ concentrations
392 measured at AF (1997 - 2015), LT (1995 - 2015) and SK (2000 - 2015). Seasonal and inter-
393 annual variability associated with changes in the prevailing meteorology and source

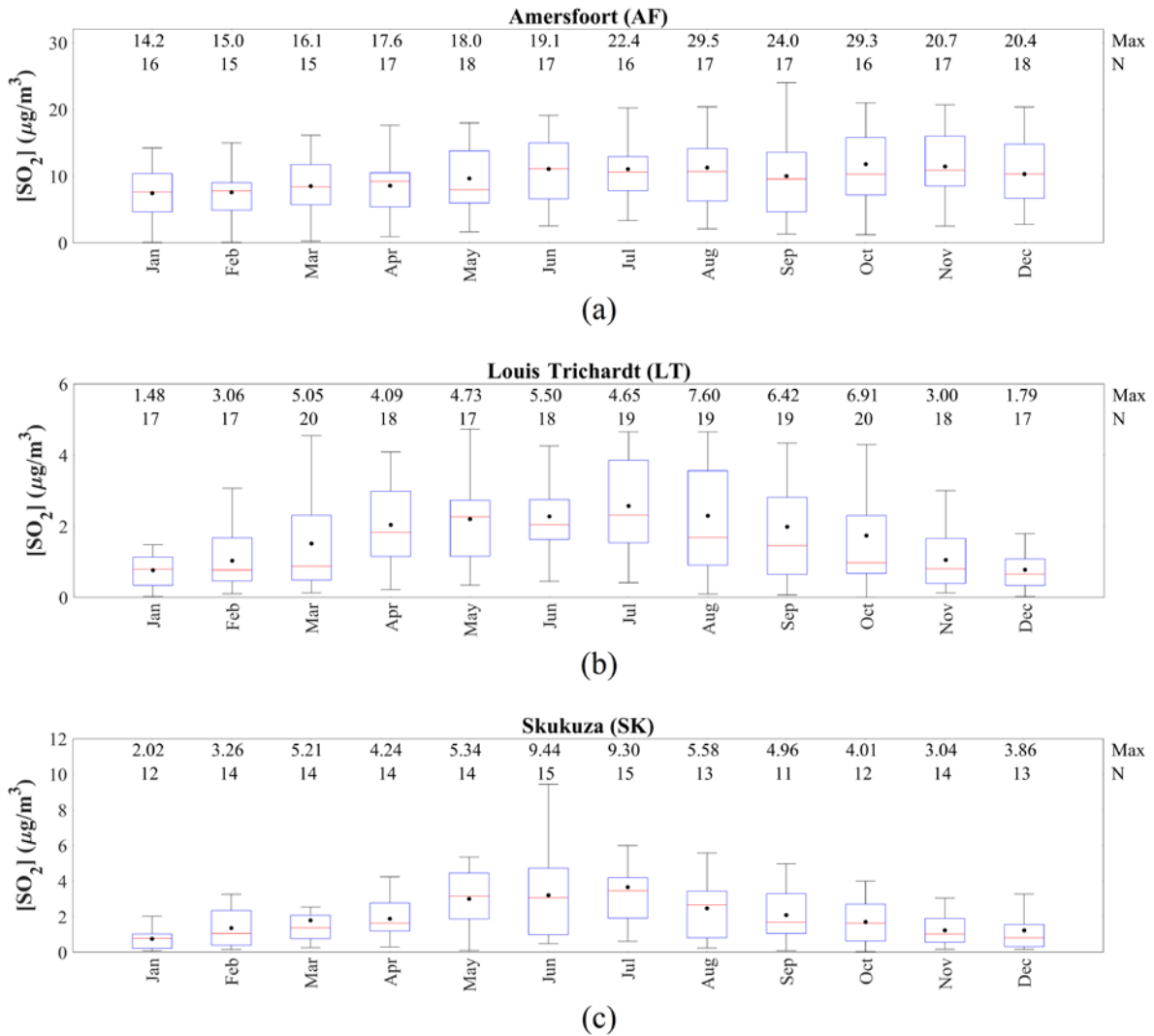
394 contributions will be evaluated and statistically assessed using multiple linear regression model
395 in subsequent sections.

396

397 **3.1 Seasonal and inter-annual variability**

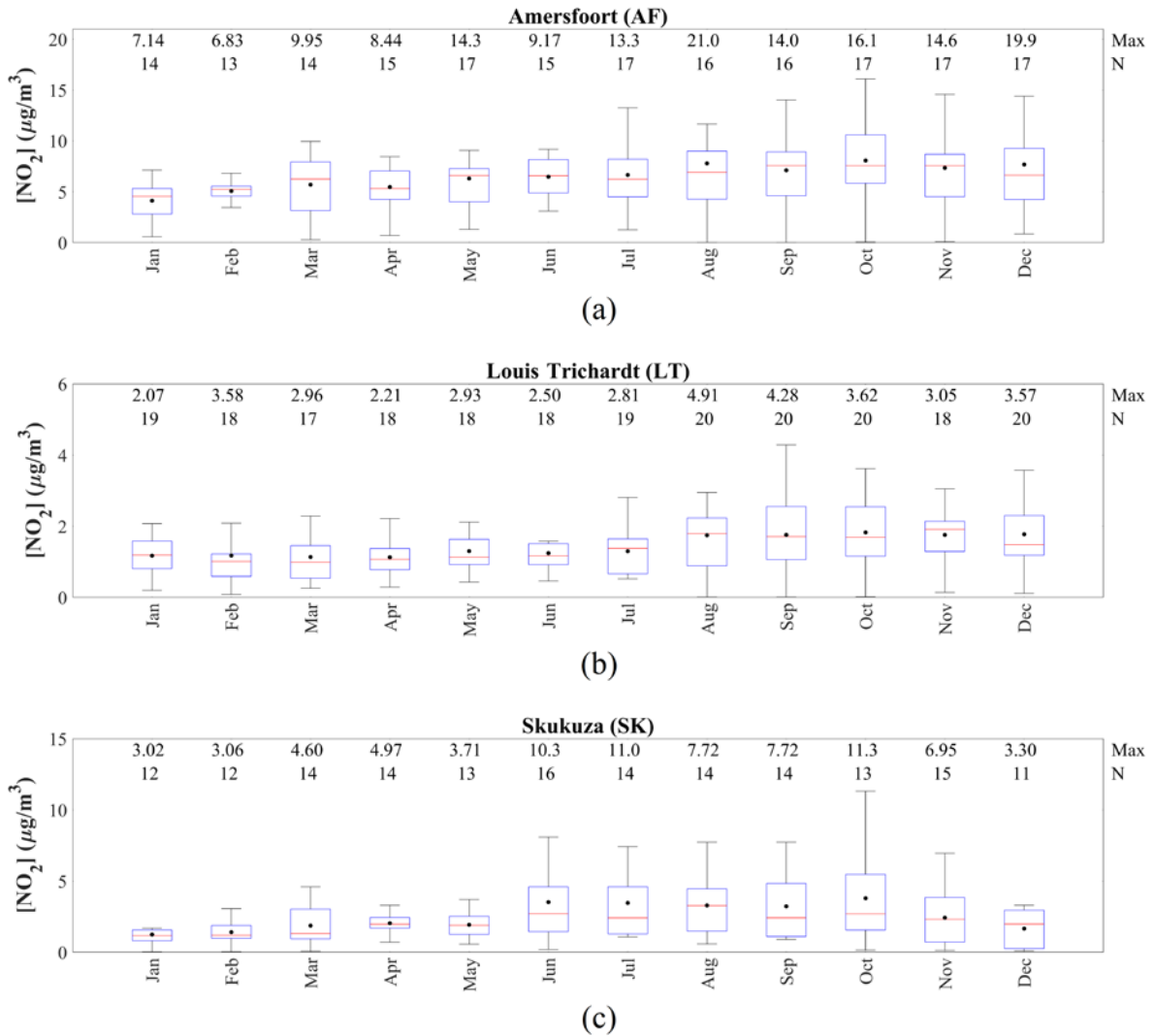
398 In Fig. 3, 4 and 5, the monthly SO₂, NO₂ and O₃ concentrations, respectively at AF, LT and
399 SK, determined for the entire sampling periods, are presented. Monthly variability in
400 concentrations of these species at these three sites is expected. The north-eastern interior of
401 South Africa, where these sites are located, is generally characterised by increased
402 concentrations in pollutant species during the dry winter months (June to September) due to
403 the prevailing meteorological conditions (Conradie et al., 2016). More pronounced inversion
404 layers trap pollutants near the surface, which, in conjunction with increased anticyclonic
405 recirculation and decreased wet deposition, leads to the build-up pollutant levels (Conradie et
406 al., 2016; Laban et al., 2018). In addition, increased household combustion for space heating
407 during winter also contributes to higher levels of atmospheric pollutants, while open biomass
408 burning (wildfires) is also a significant source of atmospheric species in late winter and spring
409 (August to November). Species typically associated with biomass burning (open or household)
410 include particulate matter (PM), CO and NO₂, while household combustion can also contribute
411 to SO₂ emissions depending on the type of fuel consumed. CO and NO₂ are also important
412 precursors of tropospheric O₃, which also lead to increased surface O₃ concentrations,
413 especially with increased photochemical activity in spring (Laban et al., 2018). From Fig. 3, it
414 is evident that SO₂ concentrations peaked in winter months at LT and SK, while SO₂ levels did
415 not reveal significant monthly variability at AF throughout the year. NO₂ and O₃ concentrations
416 at all three sites are higher during August to November, coinciding with open biomass burning.
417 NO₂ and O₃ levels at AF do not reflect the influence of pollutant build-up in winter, although
418 the whiskers in July do indicate more instances of higher NO₂ concentrations. SK did indicate
419 higher NO₂ and O₃ concentrations during June and July, while LT also had relatively higher
420 O₃ concentrations during July.

421



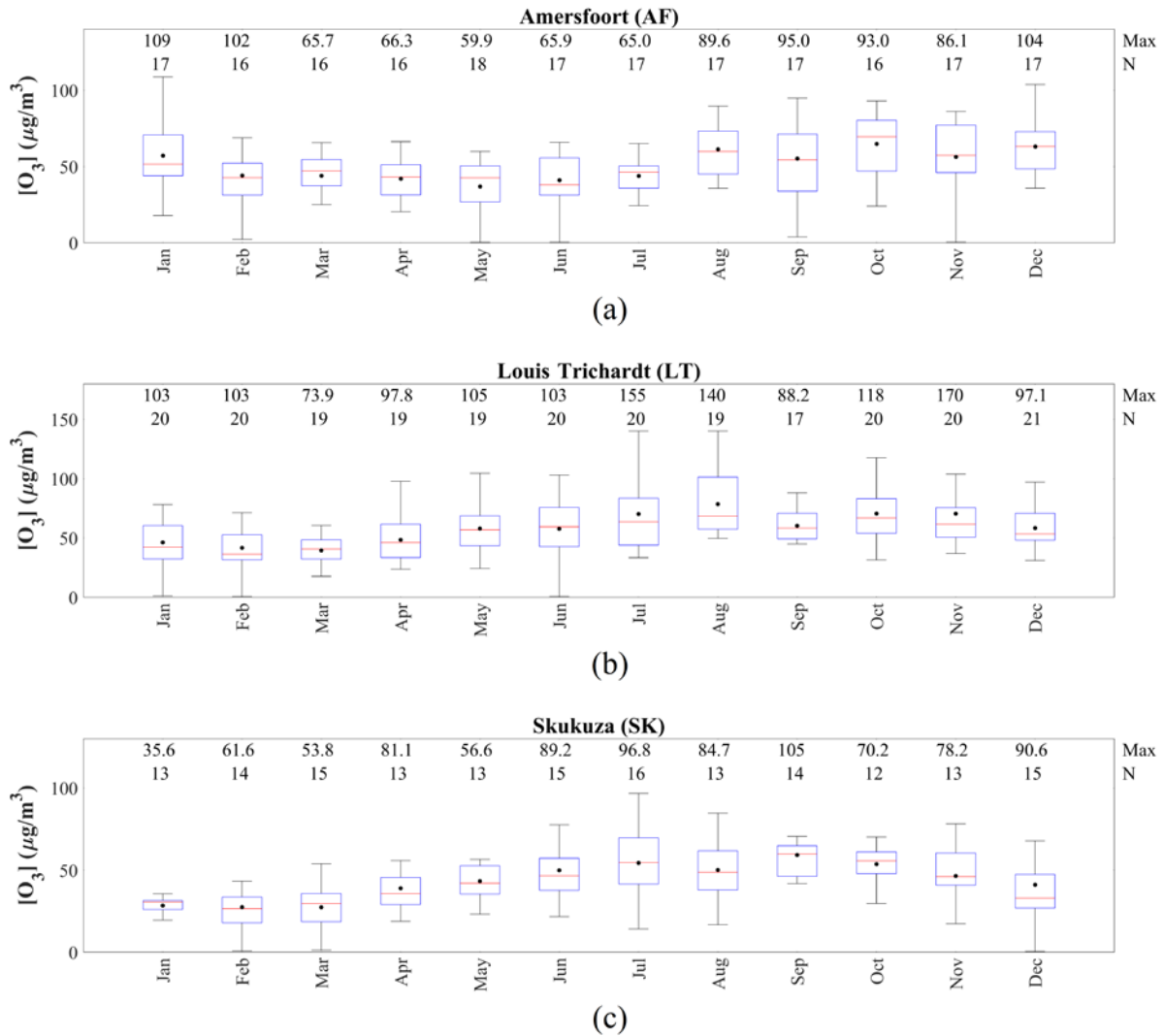
422

423 **Figure 3:** Monthly SO₂ concentrations measured at (a) AF from 1997 to 2015, (b) LT from
 424 1995 to 2015 and (c) SK from 2000 to 2015. The red line of each box represents
 425 the median, the top and bottom edges of the box the 25th and 75th percentiles,
 426 respectively, the whiskers $\pm 2.7\sigma$ (99.3% coverage if the data has a normal
 427 distribution) and the black dots the averages. The maximum concentrations and
 428 the number of measurements (N) are presented at the top



429

430 **Figure 4:** Monthly NO_2 concentrations measured at (a) AF from 1997 to 2015, (b) LT from
 431 1995 to 2015 and at (c) SK from 2000 to 2015. The red line of each box represents
 432 the median, the top and bottom edges of the box the 25th and 75th percentiles,
 433 respectively, the whiskers $\pm 2.7\sigma$ (99.3% coverage if the data has a normal
 434 distribution) and the black dots the averages. The maximum concentrations and
 435 the number of measurements (N) are presented at the top



436

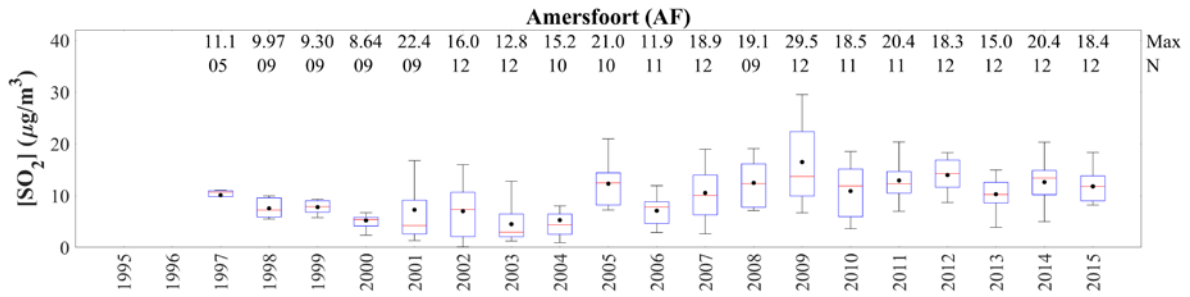
437 **Figure 5:** Monthly O₃ concentrations measured at (a) AF from 1997 to 2015, (b) LT from
 438 1995 to 2015 and (c) SK from 2000 to 2015. The red line of each box represents
 439 the median, the top and bottom edges of the box the 25th and 75th percentiles,
 440 respectively, the whiskers $\pm 2.7\sigma$ (99.3% coverage if the data has a normal
 441 distribution) and the black dots the averages. The maximum concentrations and
 442 the number of measurements (N) are presented at the top

443

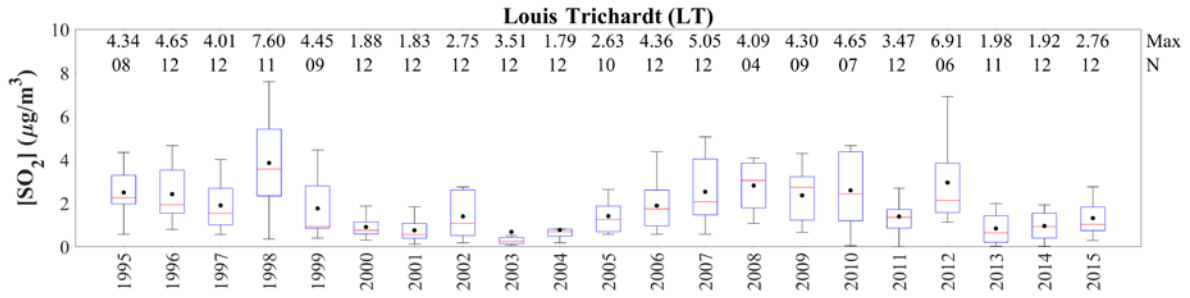
444 The inter-annual variability of SO₂, NO₂ and O₃ levels is presented in Fig. 6, 7 and 8,
 445 respectively for AF, LT and SK. Noticeable from the SO₂ and NO₂ inter-annual fluctuations at
 446 all three sites is that the annual average SO₂ and NO₂ concentrations decreased up until
 447 2003/2004 and 2002, respectively, which is followed by a period during which levels of SO₂
 448 and NO₂ increased up until 2009 and 2007, respectively. After 2009, annual average SO₂
 449 concentrations remained relatively constant, while NO₂ showed relatively large inter-annual
 450 variability, with annual NO₂ concentrations reaching a maximum in 2011 and 2012. These

451 observed periods of decreased and increased SO₂ and NO₂ levels are also indicated by the
452 three-year moving averages of the annual mean SO₂ and NO₂ concentrations at all three sites.
453 Since these trends are observed at all three sites, located several hundred kilometres apart in
454 the north-eastern interior, these inter-annual trends seem real and not merely a localised
455 artefact. Furthermore, monthly SO₂ and NO₂ measurements conducted at the Cape Point Global
456 Atmosphere Watch station on the west coast of South Africa also indicate similar periods of
457 increase and decrease in SO₂ and NO₂ levels (Swartz et al., 2020). Although annual O₃
458 concentrations indicate inter-annual variances, annual average O₃ concentrations remained
459 relatively constant at all three sites, with the exception of a decreasing trend observed from
460 1995 to 2001 at LT corresponding to the period during which SO₂ and NO₂ decreased. Similar
461 to seasonal variances, inter-annual fluctuations can also be ascribed to changes in
462 meteorological conditions and/or variances in source contribution. Conradie et al. (2016), for
463 example, indicated that rain samples collected from 2009 to 2014 at these three sites had higher
464 SO₄²⁻ and NO₃⁻ concentrations compared to rain samples collected in 1986 to 1999 and 1999
465 to 2002, which is attributed to increased energy demand and a larger vehicular fleet associated
466 with economic- and population growth.

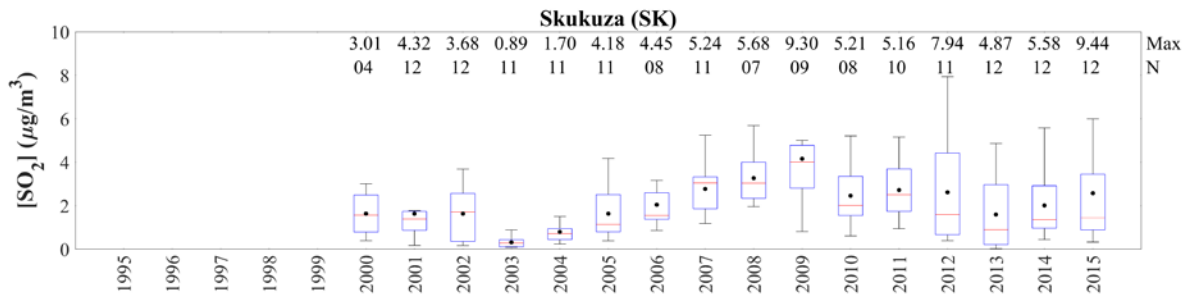
467



(a)



(b)

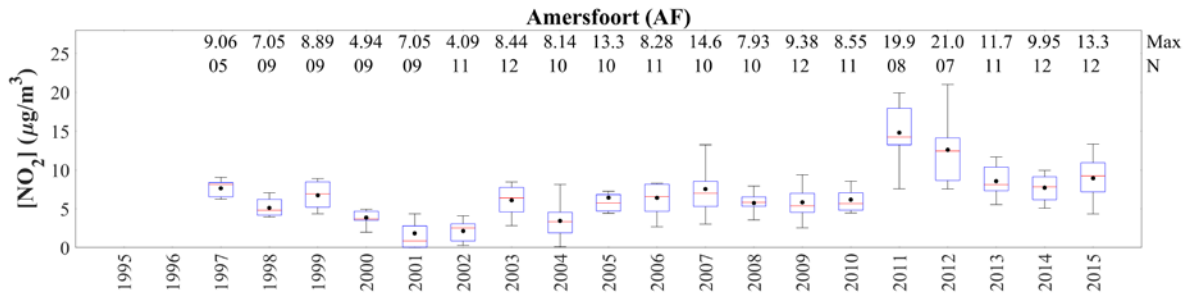


(c)

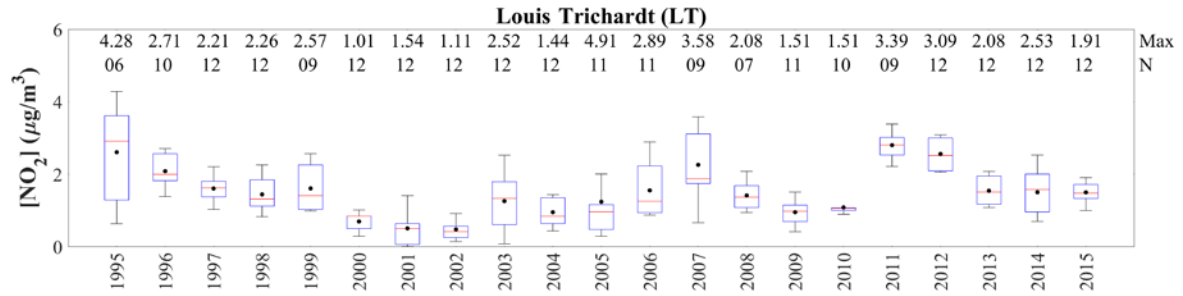
468

469 **Figure 6:** Annual SO₂ concentrations at (a) AF, (b) LT and (c) SK. The red line of each box
 470 represents the median, the top and bottom edges of the box the 25th and 75th
 471 percentiles, respectively, the whiskers $\pm 2.7\sigma$ (99.3% coverage if the data has a
 472 normal distribution) and the black dots the averages. The maximum
 473 concentrations and the number of measurements (N) are presented at the top

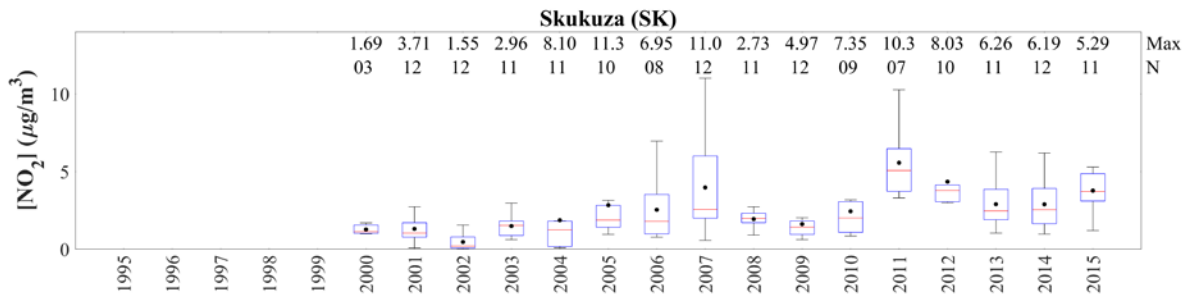
474



(a)



(b)



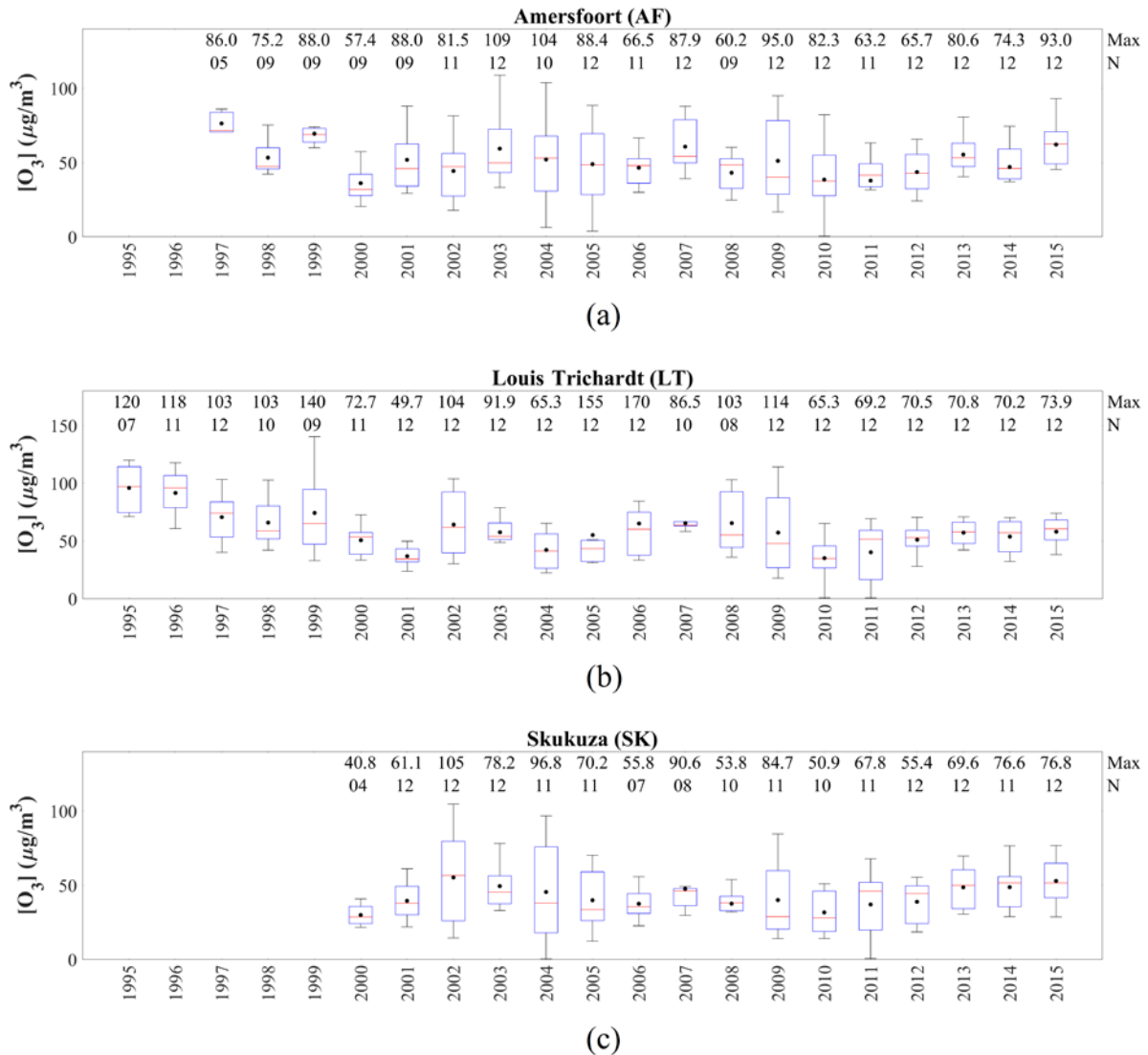
(c)

475

476 **Figure 7:** Annual NO₂ concentrations at (a) AF, (b) LT and (c) SK. The red line of each
 477 box represents the median, the top and bottom edges of the box the 25th and 75th
 478 percentiles, respectively, the whiskers $\pm 2.7\sigma$ (99.3% coverage if the data has a
 479 normal distribution) and the black dots the averages. The maximum
 480 concentrations and the number of measurements (N) are presented at the top

481

482



483

484 **Figure 8:** Annual O₃ concentrations at (a) AF, (b) LT and (c) SK. The red line of each box
 485 represents the median, the top and bottom edges of the box the 25th and 75th
 486 percentiles, respectively, the whiskers $\pm 2.7\sigma$ (99.3% coverage if the data has a
 487 normal distribution) and the black dots the averages. The maximum
 488 concentrations and the number of measurements (N) are presented at the top

489

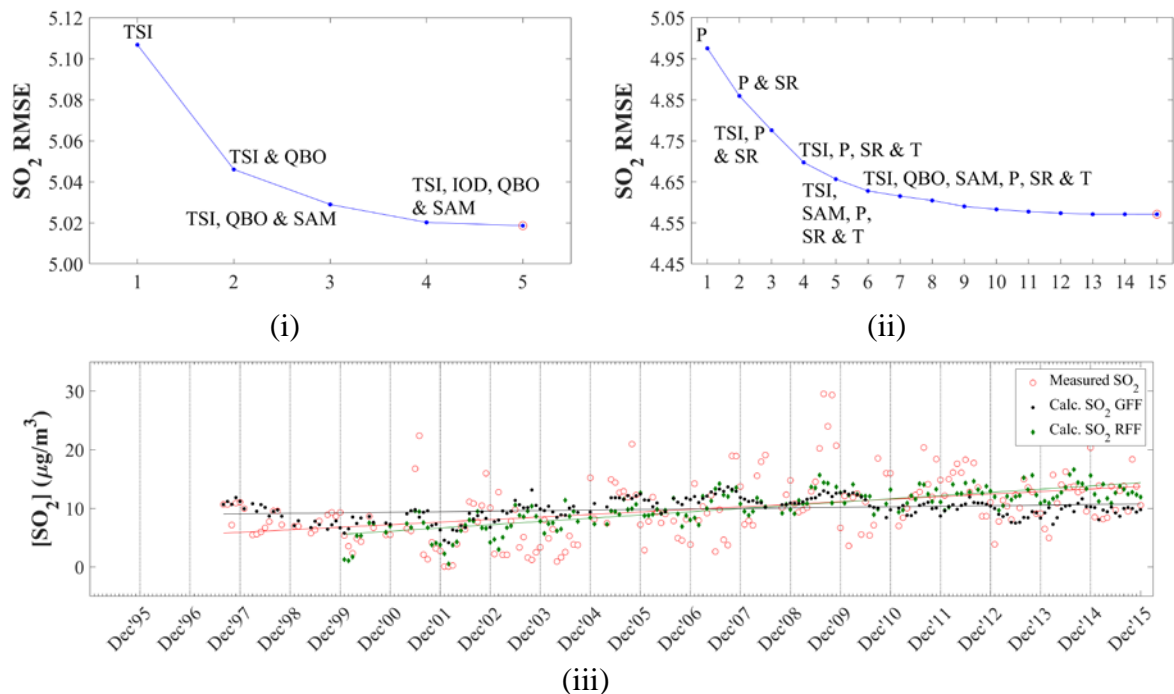
490 3.2 Statistical modelling of variability

491 3.2.1 Sulphur dioxide (SO₂)

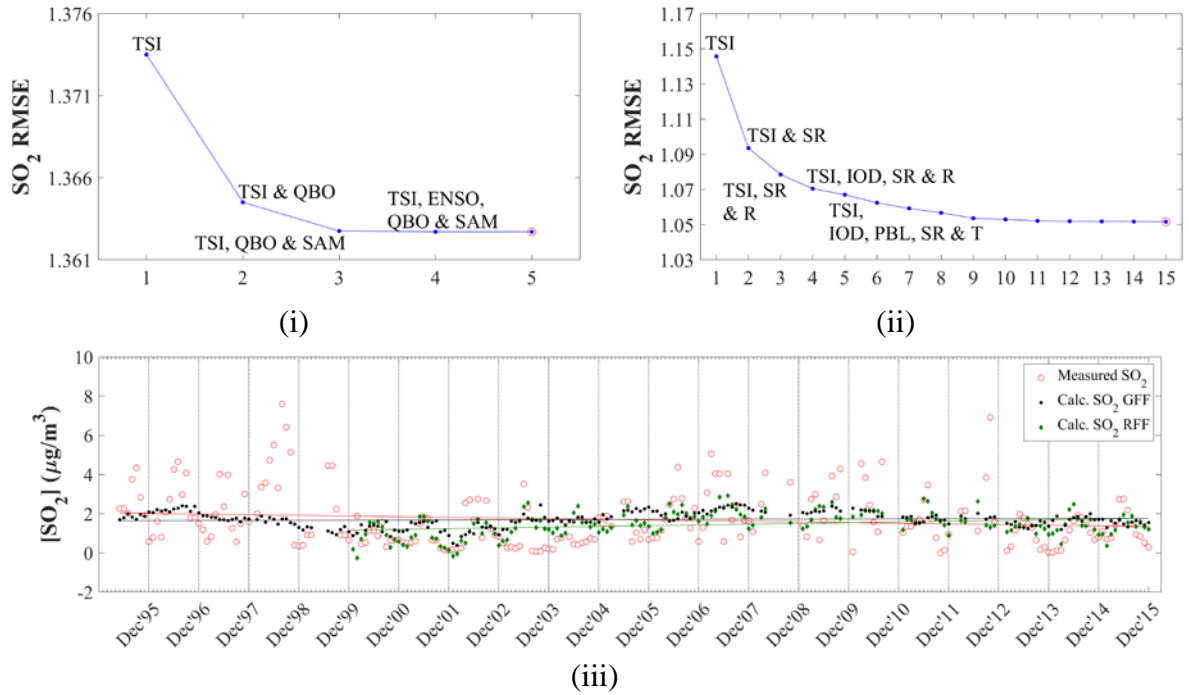
492 The SO₂ concentrations calculated with the MLR model are compared to measured SO₂ levels
 493 in Fig. 9 for AF (Fig. 9a), LT (Fig. 9b) and SK (Fig. 9c). In each sub-figure, the RMSE
 494 differences between measured and modelled SO₂ concentrations are presented as a function of
 495 the number of independent variables included in the model (i and ii), while the differences
 496 between modelled and measured SO₂ levels for each sample are also indicated (iii). As

497 indicated above, in the initial run of the model, only global factors were included (i and iii),
 498 after which all factors (local, regional and global) were incorporated in the model (ii and iii).
 499 In Table 1, the coefficients and RIW% of each of the independent variables are included in the
 500 optimum MLR equation containing all global factors, as well as in the optimum MLR equation
 501 when all local, regional and global factors are included. It is evident from Fig. 9 (iii) that the
 502 correlations between measured and modelled SO₂ levels are significantly improved when all
 503 factors are considered in the MLR model compared to only including global factors at all three
 504 sites. The R² values are improved from 0.122 to 0.330, 0.078 to 0.257, and 0.100 to 0.389 at
 505 AF, LT and SK, respectively. Although relatively weak correlations are observed between
 506 modelled and measured SO₂ levels, the general trend of the measured SO₂ concentrations is
 507 mimicked by the modelled values, even when only global factors are included in the MLR
 508 model. In addition, the R² values at AF and SK when all factors are considered (0.330 and
 509 0.389) can be considered moderate correlations (Kleynhans et al., 2017). It also seems that very
 510 high and low SO₂ levels are underestimated by the model. Swartz et al. (2020) attributed
 511 differences between monthly concentrations of species measured with passive samplers at CPT
 512 GAW and modelled levels to the limitations associated with the use of passive samplers.

513

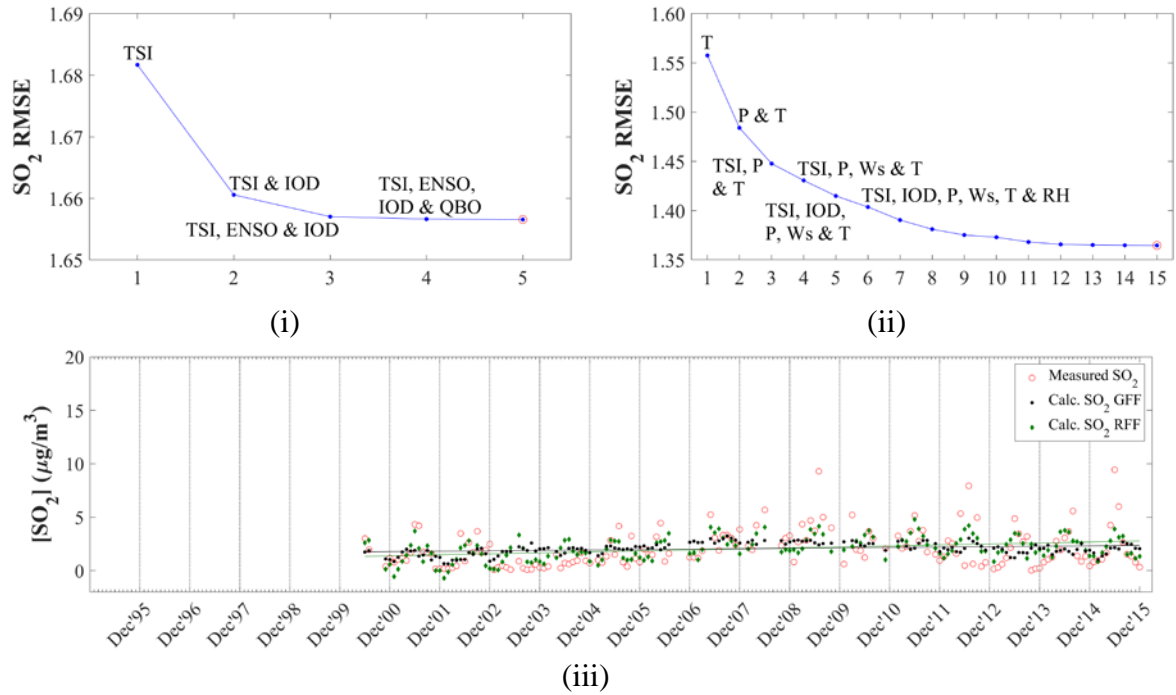


514 **Figure 9a:** (i and ii) RMSE differences between modelled and measured SO₂ concentrations
 515 as a function of the number of independent variables included in the model, as
 516 well as comparison between modelled and measured SO₂ levels (iii) for global
 517 force factors only (GFF), and for global, regional and local factors (RFF)
 518 determined for AF



519 **Figure 9b:** (i and ii) RMSE differences between modelled and measured SO₂ concentrations
 520 as a function of the number of independent variables included in the model, as
 521 well as comparison between modelled and measured SO₂ levels (iii) for global
 522 force factors only (GFF), and for global, regional and local factors (RFF)
 523 determined for LT

524



(i)

(ii)

(iii)

525 **Figure 9c:** (i and ii) RMSE differences between modelled and measured SO₂ concentrations
 526 as a function of the number of independent variables included in the model, as
 527 well as comparison between modelled and measured SO₂ levels (iii) for global
 528 force factors only (GFF), and for global, regional and local factors (RFF)
 529 determined for SK

530

531

532 **Table 1:** Regression coefficients (b) and relative important weight percentage (RIW%) of
 533 each independent variable included in the MLR model to calculate SO₂
 534 concentrations at AF, LT and SK

<u>AF</u>			<u>LT</u>			<u>SK</u>		
	<i>b</i>	<i>RIW%</i>		<i>b</i>	<i>RIW%</i>		<i>b</i>	<i>RIW%</i>
<i>i) Global forcing factors</i>								
TSI	-3.563	66.2	TSI	-0.875	80.2	TSI	-0.988	61.6
QBO	-0.057	21.2	QBO	-0.011	15.2	IOD	1.183	33.8
IOD	0.818	5.5	SAM	-0.042	3.9	ENSO	-0.158	3.7
SAM	-0.209	5.0	IOD	-0.011	0.5	QBO	-2.500×10 ⁻³	0.7
ENSO	0.170	2.0	ENSO	-0.012	0.2	SAM	-0.010	0.3
<i>ii) Global, regional and local factors</i>								
P	1.927×10 ⁻³	54.5	TSI	-0.827	34.7	T	-0.281	15.9
TSI	-2.373	14.6	SR	0.069	11.3	TSI	-0.820	12.0
SR	0.189	6.2	T	-0.109	9.9	SR	0.076	9.9
T	-0.588	4.5	IOD	0.588	8.0	P	5.610×10 ⁻⁶	9.1
QBO	-0.034	4.4	R	6.448×10 ⁻⁴	6.7	Ws	-1.357	9.1
RH	0.043	3.9	RH	-0.014	6.2	PBL	3.134×10 ⁻³	8.4
PBL	6.396×10 ⁻³	2.8	Ws	-0.404	5.1	R	9.233×10 ⁻⁴	7.4
SAM	-0.406	2.6	PBL	1.520×10 ⁻³	4.9	RH	-0.024	7.0
R	-1.104×10 ⁻³	1.8	Wd	2.746×10 ⁻³	3.1	IOD	1.011	6.7
Ws	0.076	1.5	P	-1.035×10 ⁻⁶	2.7	Wd	-4.034×10 ⁻⁴	5.6
IOD	-0.674	0.9	SAM	-0.049	2.4	LFE	5.827×10 ⁻⁵	4.5
LFE	1.114×10 ⁻⁴	0.9	DFE	-2.892×10 ⁻⁷	2.0	DFE	-3.355×10 ⁻⁶	2.2
Wd	-3.502×10 ⁻³	0.6	QBO	-6.471×10 ⁻³	1.6	ENSO	-0.260	1.7
DFE	-1.319×10 ⁻⁵	0.5	LFE	-8.706×10 ⁻⁵	0.8	SAM	-0.078	0.5
ENSO	-0.310	0.3	ENSO	-0.034	0.6	QBO	-2.726×10 ⁻³	0.2

535

536 The interdependencies between TSI and QBO at AF and LT, as well as TSI and IOD at SK
 537 yielded the largest decreases in RMSE when only global parameters were considered. The
 538 RIW% calculated for these parameters in the optimum MLR equation containing all global
 539 factors also indicates that these factors are the most significant. When all factors (local, regional
 540 and global) were considered in the model, the combinations between P, TSI, SR and T at AF,
 541 TSI, SR, IOD and R at LT, and T, TSI, P and Ws contributed to the most significant decrease
 542 in RMSE for each of the sites. According to the RIW% calculated for each parameter in the
 543 optimum MLR equation containing all factors P (54.5%) and TSI (14.6%) at AF, TSI (34.7%),
 544 SR (11.3%), T (9.9%) and IOD (8.0%) at LT, and T (15.9%), TSI (12.0%), SR (9.9%), P (9.1%)
 545 and Ws (9.1%) at SK were the most important factors contributing to variances. From the MLR

546 model, it is evident that global meteorological factors contribute to SO₂ variability at each of
547 these sites located in the north-eastern interior of South Africa. The model also indicates that
548 the influence of global factors is more significant at the rural background site LT, where TSI
549 made the largest contribution to the modelled value, while IOD also made a relatively important
550 contribution. Although TSI was the second most significant factor at AF and SK, local and
551 regional parameters were more important to variances in modelled SO₂ levels at these sites.

552 Population growth had the most substantial contribution to the dependent variable at the
553 industrially influenced AF, which is indicative of the impacts of increased anthropogenic
554 activities and energy demand in this region. Therefore, it is most-likely that the observed inter-
555 annual variability observed at AF, i.e. periods of decreased and increased SO₂ levels, can
556 mainly be attributed to changes in source contribution. The decrease in SO₂ concentrations up
557 until 2003/2004 is associated with a period post-1994 (when the new democracy was
558 established) during which many companies obtained environmental accreditation (ISO 14000
559 series, ISO survey, 2015) and implemented mitigation technologies in order to comply with
560 international trade requirements, e.g. certain large metallurgical smelters applied
561 desulphurisation technologies (e.g. Westcott et al., 2007). The period was characterised by an
562 increased awareness of air pollution and its impacts in South Africa. However, it seems that
563 these improvements made with regard to air pollution were offset from 2003/2004 due to rapid
564 economic growth associated with increased industrial activities, e.g. increased production by
565 pyrometallurgical industries (ICDA, 2012), as well as the increase in population growth
566 accompanied by higher energy demand (Vet et al., 2014). [In Fig. A4, the South African
567 population and GDP from 1995 to 2015 according to the World Bank \(World Bank, 2019\) are
568 presented together with the electricity generation \(EG\) in South Africa during this period as
569 indicated by the International Energy Agency \(International Energy Agency, 2020\). A
570 continuous growth in population is observed from 1995 to 2015, while the GDP trend reflects
571 economic growth during this period corresponding to the observed periods of decreased and
572 increased SO₂ concentrations. A general increase in electricity production over this period is
573 also evident.](#) Electricity consumption is a good indicator of increased anthropogenic activities,
574 with Inglesi-Lotz and Blignaut (2011) indicating that electricity consumption in South Africa
575 increased by 131 024 GWh from 1993 to 2006. In 2007/2008, the global financial crisis
576 occurred, which forced numerous South African commodity-based producers (e.g. platinum
577 group metal, base metal, ferrochromium, ferromanganese, ferrovanadium and steel smelters)
578 to completely discontinue production. Ferrochromium production in South Africa, for instance,

579 decreased by approximately 35% from 2007 to 2009 (ICDA, 2013), while energy consumption
580 in the manufacturing sector dropped by approximately 34% from 2007 to 2008 (Statistics South
581 Africa, 2012). Furthermore, these variances in source contribution associated with
582 anthropogenic activities are also observed at LT and SK distant from the major sources due to
583 these sites also being impacted by the regional circulation of air masses passing over major
584 sources, as indicated in Fig. 2. In addition, the RIW% associated with P (9.1%) in the optimum
585 MLR equation containing all factors at SK is also indicative of not only the influence of
586 population growth within the source region (Fig. 1), but also the increased populations of rural
587 communities on the border of the Kruger National Park. Maritz et al. (2020) attributed higher
588 organic- and elemental carbon concentrations measured at SK to increased household biomass
589 burning by these rural communities.

590 Temperature had the largest contribution to the variances of the modelled SO₂ at SK, while it
591 was also an important parameter at LT. In addition, the source region (SR) factor made
592 significant contributions to the dependent variable at SK and LT, while it also made a relative
593 contribution at AF. These two factors are indicative of the influence of changes in local and
594 regional meteorological conditions on SO₂ concentrations, as well as the important influence
595 of air mass movement over the source region. The contribution of SR at all the sites indicated
596 that months and/or years coinciding with these sites being more frequently impacted by air
597 masses passing over the defined source region (Fig. 1) corresponded to increased SO₂
598 concentrations, while it also substantiates the afore-mentioned deduction that increased
599 anthropogenic activities in the source region also influenced LT and SK. As indicated in section
600 3.1, SK and LT revealed the expected higher SO₂ levels during winter, while AF had a less
601 distinct seasonal pattern. Therefore, the strong negative correlation between temperature and
602 modelled SO₂ concentrations at SK and LT, i.e. higher SO₂ levels associated with lower
603 temperature, reflects the influence of local and regional meteorology on monthly SO₂
604 variability, i.e. build-up of pollutant concentrations during winter. At SK, the influence of local
605 meteorology is also indicated by the relative strong negative correlation to Ws, i.e. more stable
606 conditions in winter coinciding with higher SO₂ concentrations. Furthermore, the influence of
607 the rural communities in proximity of SK on SO₂ levels is also signified by T being the most
608 significant factor contributing to modelled SO₂ values at this site. The less distinct seasonal
609 pattern at AF can be attributed to the proximity of AF to the industrial SO₂ sources, with the
610 major point sources consistently emitting the same levels of SO₂ throughout the year.

611 Therefore, the average monthly SO₂ concentrations measured with passive samplers at AF do
612 not reflect the influence of local and regional meteorology on atmospheric SO₂ concentrations.

613 The slopes of the trend lines of SO₂ values calculated when only global factors were included
614 in the model did not correspond with the trend lines of the measured SO₂ concentrations at all
615 the sites, with the exception of LT that showed slightly better correlations, signifying the
616 stronger influence of global factors at this site (Pane iii in Fig. 9a, b and c). However, the slopes
617 of the linear regression trend lines for the measured SO₂ concentrations and the modelled SO₂
618 levels when all the factors are included in the model are exactly the same at AF, LT and SK
619 when the same period is considered for both the modelled and measured values. A positive
620 slope for the 19-year trend line for measured SO₂ concentrations is observed at AF (Fig. 9a(iii)),
621 indicating an increase in SO₂ levels over the 19-year sampling period, i.e. 0.43 µg.m⁻³.y⁻¹. An
622 increase in SO₂ concentration, i.e. 0.09 µg.m⁻³.y⁻¹ is also determined for the 16-year
623 measurement period at SK (Fig. 9b(iii)), which is significantly smaller than the upwards trend
624 at AF. In contrast to AF and SK, LT indicates a slight net negative slope with SO₂ decreasing
625 on average by 0.03 µg.m⁻³.y⁻¹ during the 21-year sampling period (Fig. 9c(iii)). The 19- and
626 21-year datasets at AF and LT also allowed for the calculation of decadal trends, which were
627 determined to be 5.24 µg.m⁻³.dec⁻¹ (average SO₂ concentrations from 1997 to 2006 were 7.20
628 µg.m⁻³ and average SO₂ concentrations from 2007 to 2015 were 12.44 µg.m⁻³) and 0.18 µg.m⁻³.
629 dec⁻¹ (average SO₂ concentrations from 1995 to 2004 were 1.64 µg.m⁻³ and average SO₂
630 concentrations from 2005 to 2014 were 1.82 µg.m⁻³), respectively, for the two decades. Trend
631 lines are also presented for the periods characterised by increased (1995, 1997 to 2003) and
632 decreased (2004 to 2008/2009) SO₂ concentrations at LT and AF. The average annual trend
633 between 1997 and 2003 at AF was -0.53 µg.m⁻³.y⁻¹, while the annual trend from 2004 to 2009
634 was 1.87 µg.m⁻³.y⁻¹. At LT, the average annual SO₂ concentrations decreased by -0.26 µg.m⁻³.
635 y⁻¹ from 1995 to 2002, and increased by 0.37 µg.m⁻³.y⁻¹ from 2003 to 2007.

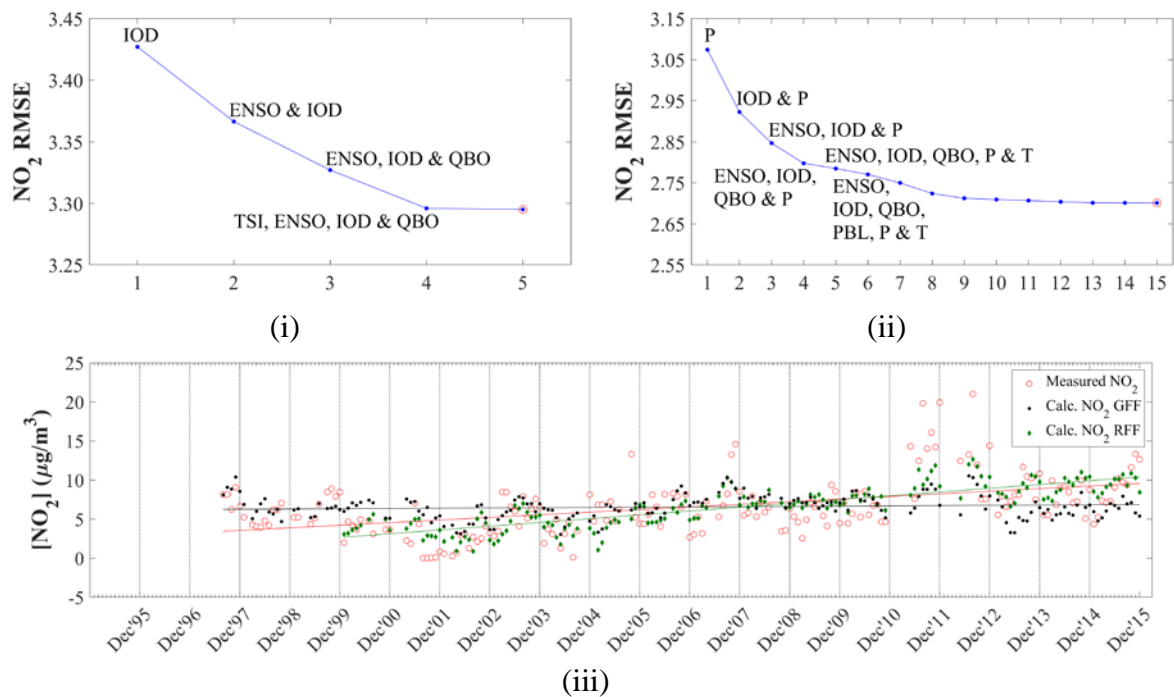
636

637 **3.2.2 Nitrogen dioxide (NO₂)**

638 In Fig. 10, the measured NO₂ concentrations are related to the modelled NO₂ levels, while
639 Table 2 presents the coefficients and RIW% of each of the independent variables included in
640 the optimum MLR equation modelling NO₂ concentrations. Similar to SO₂, the relationships
641 between measured and modelled NO₂ are also significantly improved when local, regional and
642 global factors are included in the model at all three sites (Pane iii in Fig. 10a, b and c). However,

643 inclusion of only global factors in the model yielded modelled NO₂ concentrations that
 644 mimicked the general measured NO₂ trend. The R² values, when only global factors are
 645 included, i.e. 0.171, 0.170 and 0.099 at AF, LT and SK, respectively, are enhanced to 0.498,
 646 0.468 and 0.362 at AF, LT and SK, respectively, when all factors are considered in the MLR
 647 model. The R² values, when all factors are included, especially AF and LT, can be considered
 648 relatively good correlations (Sheskin, 2003). In general, modelled NO₂ concentrations
 649 corresponded well with the observed variances in measured NO₂ levels when all factors are
 650 included in the model at all three sites, with the exception of very high NO₂ concentrations.

651



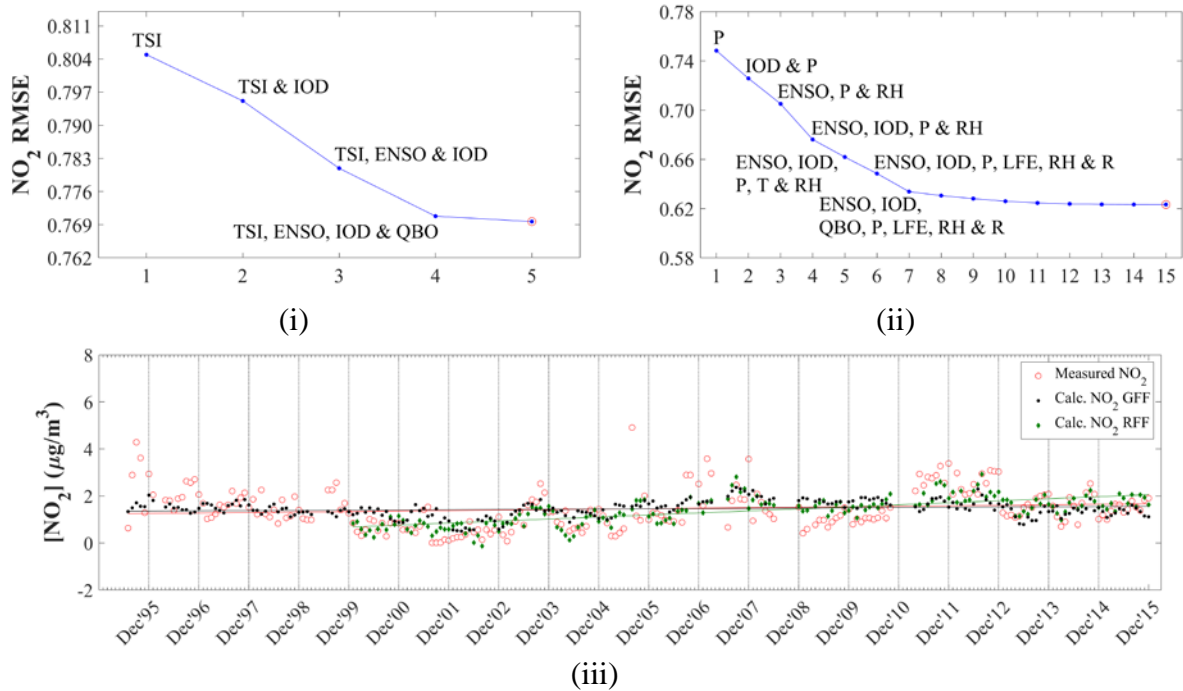
652 **Figure 10a:** (i and ii) RMSE differences between modelled and measured NO₂ concentrations
 653 as a function of the number of independent variables included in the model, as
 654 well as comparison between modelled and measured NO₂ levels (iii) for global
 655 force factors only (GFF), and for global, regional and local factors (RFF)
 656 determined for AF

657

658

659

660



(i)

(ii)

(iii)

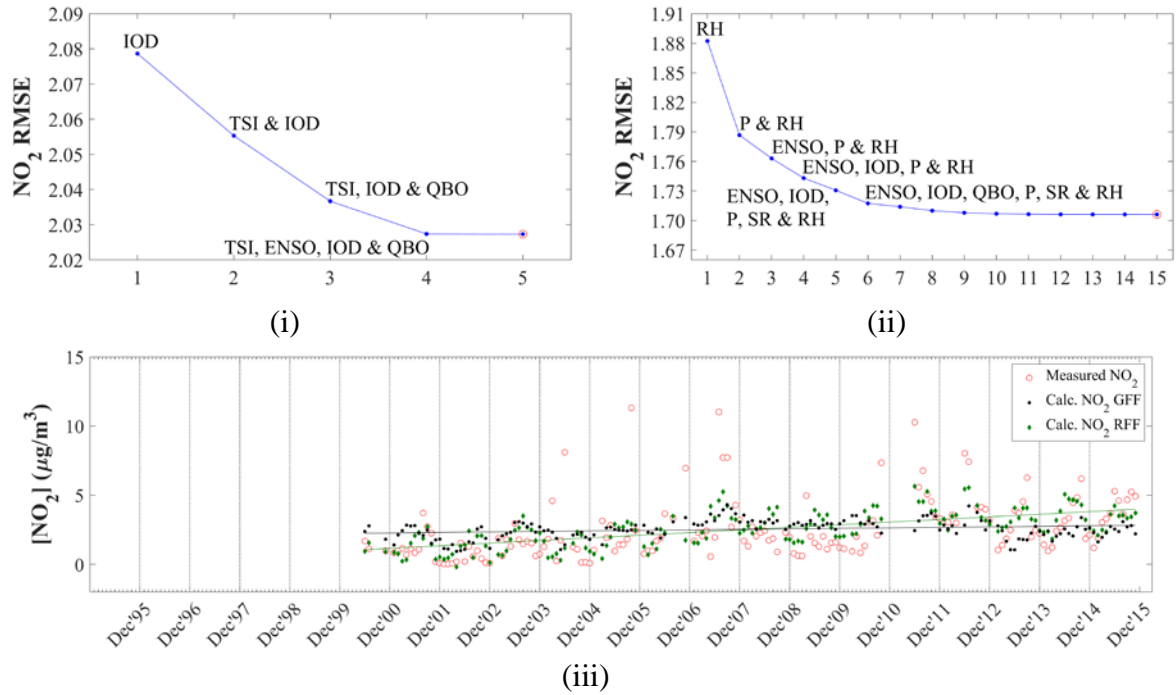
661 **Figure 10b:** (i and ii) RMSE differences between modelled and measured NO₂ concentrations
 662 as a function of the number of independent variables included in the model, as
 663 well as comparison between modelled and measured NO₂ levels (iii) for global
 664 force factors only (GFF), and for global, regional and local factors (RFF)
 665 determined for LT

666

667

668

669



670 **Figure 10c:** (i and ii) RMSE differences between modelled and measured NO₂ concentrations
 671 as a function of the number of independent variables included in the model, as
 672 well as comparison between modelled and measured NO₂ levels (iii) for global
 673 force factors only (GFF), and for global, regional and local factors (RFF)
 674 determined for SK

675

676 **Table 2:** Regression coefficients (b) and relative important weight percentage (RIW%) of
 677 each independent variable included in the MLR model to calculate NO₂
 678 concentrations at AF, LT and SK

<u>AF</u>			<u>LT</u>			<u>SK</u>		
	<i>b</i>	<i>RIW%</i>		<i>b</i>	<i>RIW%</i>		<i>b</i>	<i>RIW%</i>
<i>i) Global forcing factors</i>								
IOD	4.718	65.3	TSI	-0.625	52.4	IOD	1.954	49.4
TSI	-1.156	15.1	IOD	0.723	25.5	TSI	-0.698	27.6
QBO	-0.037	10.5	QBO	-9.326×10 ⁻³	11.8	QBO	-0.018	15.4
ENSO	-0.798	8.6	ENSO	-0.186	8.9	ENSO	-0.301	7.1
SAM	0.047	0.5	SAM	0.025	1.4	SAM	-8.422×10 ⁻³	0.5
<i>ii) Global, regional and local factors</i>								
P	1.444×10 ⁻³	53.7	P	1.512×10 ⁻⁵	29.9	P	1.366×10 ⁻⁵	29.8
IOD	3.861	17.8	RH	-0.056	16.6	RH	-0.090	20.6
RH	-0.036	6.0	IOD	0.916	15.2	IOD	1.032	7.1
QBO	-0.028	3.5	TSI	-0.186	8.4	DFE	1.473×10 ⁻⁷	6.9
PBL	5.119×10 ⁻³	3.2	ENSO	-0.327	6.8	R	3.833×10 ⁻³	6.1
TSI	0.040	2.8	QBO	-9.368×10 ⁻³	6.5	LFE	3.800×10 ⁻⁶	4.1
ENSO	-0.965	2.7	R	2.482×10 ⁻³	3.8	SR	0.073	4.0
Ws	0.075	2.7	DFE	-6.055×10 ⁻⁷	2.9	T	-0.072	3.8
T	-0.415	2.5	PBL	-1.225×10 ⁻³	2.5	TSI	-0.160	3.7
R	0.014	1.5	T	0.069	1.9	QBO	-0.015	3.6
LFE	-1.229×10 ⁻⁴	1.0	LFE	-2.134×10 ⁻⁴	1.8	ENSO	-0.441	3.1
DFE	-5.044×10 ⁻⁶	0.9	Ws	0.107	1.5	Ws	0.313	3.0
SR	0.028	0.6	SAM	0.021	0.8	Wd	4.912×10 ⁻⁴	1.9
Wd	-1.419×10 ⁻³	0.6	SR	0.010	0.8	PBL	1.567×10 ⁻⁴	1.8
SAM	-0.141	0.5	Wd	-1.587×10 ⁻⁴	0.6	SAM	-0.025	0.5

679

680 The annual trend calculated from the slope of the 19-year measured NO₂ dataset at AF indicates
 681 an annual increase of 0.33 µg.m⁻³.y⁻¹, while the 16-year measured NO₂ concentrations indicate
 682 an upwards trend of 0.19 µg.m⁻³.y⁻¹ at SK. The trend line of measured NO₂ concentrations at
 683 LT also indicated a marginal increase, i.e. 0.02 µg.m⁻³.y⁻¹ in NO₂ levels over the 21-year
 684 sampling period. Decadal trends were determined to be 3.43 µg.m⁻³.dec⁻¹ (average NO₂
 685 concentrations from 1997 to 2006 were 4.86 µg.m⁻³ and average NO₂ concentrations from 2007
 686 to 2015 were 8.29 µg.m⁻³) and 0.45 µg.m⁻³.dec⁻¹ (average NO₂ concentrations from 1995 to
 687 2004 were 1.23 µg.m⁻³ and average NO₂ concentrations from 2005 to 2014 were 1.68 µg.m⁻³),
 688 respectively, for the two decades. Trend lines were also calculated for the periods coinciding
 689 with increases and decreases in measured NO₂ concentrations at AF and LT. The average

690 annual trend between 1997 and 2003 at AF was $-0.26 \mu\text{g}\cdot\text{m}^{-3}\cdot\text{y}^{-1}$, while the annual trend from
691 2004 to 2009 was $0.37 \mu\text{g}\cdot\text{m}^{-3}\cdot\text{y}^{-1}$. At LT, the average annual NO_2 concentrations decreased by
692 $-0.29 \mu\text{g}\cdot\text{m}^{-3}\cdot\text{y}^{-1}$ from 1995 to 2002, and increased by $0.28 \mu\text{g}\cdot\text{m}^{-3}\cdot\text{y}^{-1}$ from 2003 to 2007. Similar
693 to SO_2 , the slopes of the linear regression trend lines for the measured NO_2 concentrations and
694 the modelled NO_2 levels when all the factors are included in the model are exactly the same at
695 AF, LT and SK (Pane iii in Fig. 10a, b and c). However, with the exception of LT, the slopes
696 of the trend lines of NO_2 levels calculated including only global factors in the model did not
697 correspond with the trend lines of the measured NO_2 concentrations, indicating the significance
698 of local and regional factors on measured NO_2 concentrations (Pane iii in Fig. 10a, b and c).

699 The RMSE differences between the modelled and measured NO_2 concentrations (Pane i Fig.
700 10a, b and c) indicated that the linear combination between most of the global force factors,
701 i.e. IOD, TSI, QBO and ENSO, resulted in the largest decrease in RMSE when only global
702 force factors were included. The RIW% listed in Table 2 for the optimum MLR equation,
703 including only global factors, indicates that IOD (65.3% and 49.4%, respectively) was the most
704 significant parameter at AF and SK, while TSI (52.4%) was the most important factor at LT.
705 The inclusion of local, regional and global factors in the MLR model indicated that the
706 interdependencies between P, IOD, QBO, ENSO and T at AF, P, RH, IOD, ENSO and T at
707 LT, and P, RH, IOD and ENSO at SK, yielded the largest decrease in RMSE difference. The
708 RIW% determined for each independent variable in the optimum MLR equation containing all
709 parameters indicated the most important factors explaining variances in the dependent variable
710 (i.e. NO_2 levels) were P (53.7%) and IOD (17.8%) at AF, P (29.9%), RH (16.6%) and IOD
711 (15.5%) at LT, and P (29.8%) and RH (20.6%) at SK. It is evident from these interdependencies
712 of the dependent variable and RIW% of parameters included in the MLR model that local and
713 regional factors were more significant to NO_2 variability at AF, LT and SK, while global
714 meteorological factors also contributed to variances in NO_2 levels.

715 Population growth made the most significant contribution to modelled NO_2 concentrations at
716 all three sites, and not only at AF, as observed for SO_2 . Therefore, the influence of increased
717 population growth and associated anthropogenic activities is reflected in ambient NO_2
718 concentrations modelled for the entire north-eastern interior region. Therefore, the periods
719 coinciding with decreased (up until 2002) and increased (2003 to 2007) NO_2 inter-annual
720 variability can be attributed to similar variances in source contribution, as discussed above for
721 SO_2 , with regional circulation of air masses passing over major sources also influencing LT
722 and SK (Fig. 2). However, the significant contribution of population growth to the modelled

723 NO₂ levels at two rural background sites (LT and SK) also points to increased household
724 combustion associated with enlarged populations within rural communities being a major
725 source of NO₂ in this part of South Africa. The influence of increased seasonal household
726 combustion is also indicated by higher NO₂ concentrations determined in June and July at SK
727 (Fig. 4), which also signifies the impacts of the growing rural communities in proximity of SK.

728 RH made the second most important contribution in explaining variances in modelled NO₂
729 concentrations at LT and SK, while it was the third most important factor at AF as indicated
730 by RIW%. Therefore, RH can be considered the factor representing the influence of changes
731 in local and regional meteorology at these sites. Although T was indicated as a factor included
732 in the linear combination of parameters yielding the largest decrease in RMSE at AF and SK,
733 its relative importance in explaining modelled variances is not indicated by its RIW% in Table
734 2. The strong negative correlation with RH is indicative of increased NO₂ corresponding with
735 months (or years) when dry meteorological conditions prevail, i.e. winter and early spring
736 months in the north-eastern interior of South Africa. As indicated in Fig. 4, higher NO₂
737 concentrations did correspond with dry months (August to November) associated with
738 increased biomass burning. However, the model does not reflect significant contributions of
739 the two parameters included in the model to represent biomass burning, i.e. LFE and DFE to
740 NO₂ variability with relatively higher RIW% observed for DFE (6.9%) and LFE (4.1%) only
741 at SK. Furthermore, higher annual average NO₂ concentrations observed in 2011 and 2012
742 (Fig. 7) at all the sites are also not explained by the MLR model.

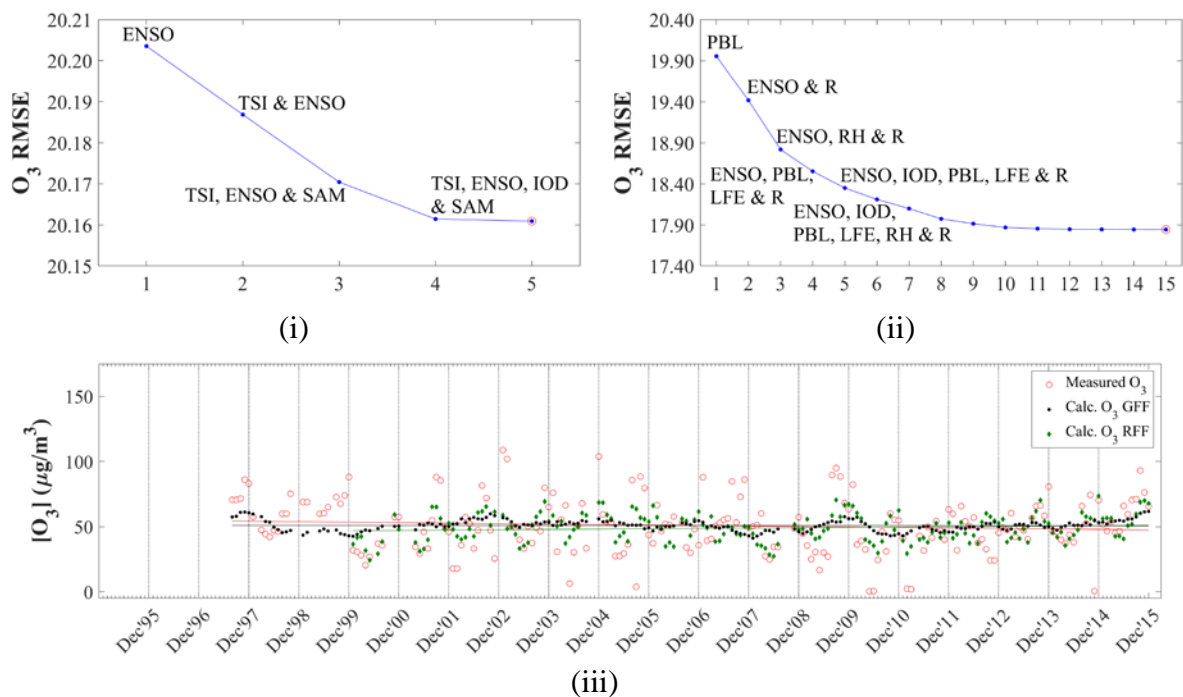
743

744 **3.2.3 Ozone (O₃)**

745 Modelled and measured O₃ concentrations at AF, LT and SK are presented in Fig.11, while
746 Table 3 presents the coefficients and the RIW% of independent variables considered in the
747 optimum MLR equation. When only global factors are considered in the model, the linear
748 combinations between ENSO, TSI, IOD and SAM at AF, ENSO, TSI and SAM at LT, and
749 ENSO and IOD at SK resulted in the largest RMSE differences between measured and
750 modelled O₃ levels. However, according to RIW% values calculated, the most significant
751 global factor contributing to O₃ variability was ENSO at all three sites (84.1%, 41.8% and
752 96.7% at AF, LT and SK, respectively). The interdependencies between parameters when local,
753 regional and global factors were included in the models, as well as the RIW% contributions of
754 all factors included in the optimum MLR equation also indicated the significance of ENSO in

755 explaining variances in atmospheric O₃ concentrations at all three sites. Interdependencies
 756 between ENSO, IOD, PBL, LFE and R at AF, ENSO, PBL, T, RH and R at LT, and ENSO,
 757 PBL, T, RH and R at SK yielded the largest decrease in RMSE differences between measured
 758 and modelled O₃ levels, while RIW% indicated that the largest contributions made by factors
 759 explaining O₃ variability were ENSO (22.6%), R (14.6%) and Ws (10.1%) at AF, RH (23.1%),
 760 ENSO (16.8%) and T (10.5%) at LT, and T (24.6%), ENSO (19.5%), RH (11.3%) and DFE
 761 (10.1%) at SK when local, regional and global factors were included in the model.

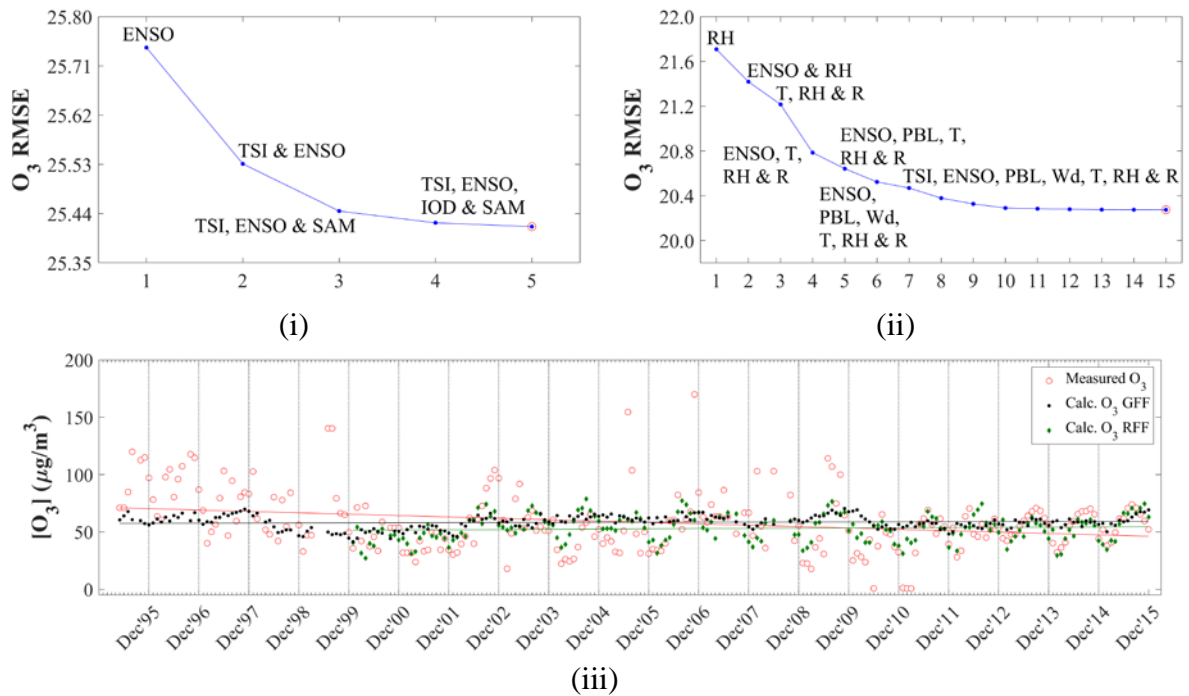
762



763 **Figure 11a:** (i and ii) RMSE differences between modelled and measured O₃ concentrations
 764 as a function of the number of independent variables included in the model, as
 765 well as comparison between modelled and measured O₃ levels (iii) for global
 766 force factors only (GFF), and for global, regional and local factors (RFF)
 767 determined for AF

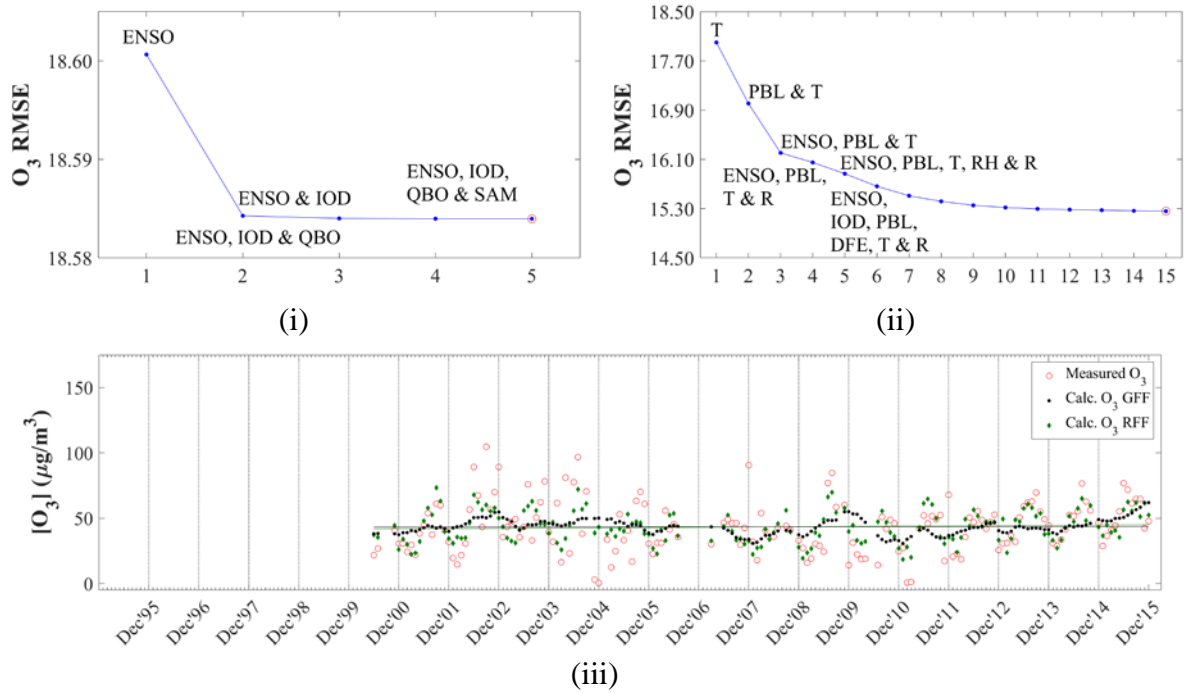
768

769



770 **Figure 11b:** (i and ii) RMSE differences between modelled and measured O₃ concentrations
 771 as a function of the number of independent variables included in the model, as
 772 well as comparison between modelled and measured O₃ levels (iii) for global
 773 force factors only (GFF), and for global, regional and local factors (RFF)
 774 determined for LT

775
 776
 777
 778



779 **Figure 11c:** (i and ii) RMSE differences between modelled and measured O₃ concentrations
 780 as a function of the number of independent variables included in the model, as
 781 well as comparison between modelled and measured O₃ levels (iii) for global
 782 force factors only (GFF), and for global, regional and local factors (RFF)
 783 determined for SK

784

785

786 **Table 3:** Regression coefficients (b) and relative important weight percentage (RIW%) of
 787 each independent variable included in the MLR model to calculate O₃
 788 concentrations at AF, LT and SK

	<u>AF</u>		<u>LT</u>		<u>SK</u>			
	<i>b</i>	<i>RIW%</i>	<i>b</i>	<i>RIW%</i>	<i>b</i>	<i>RIW%</i>		
<i>i) Global forcing factors</i>								
ENSO	4.923	84.1	ENSO	4.732	41.8	ENSO	8.353	96.7
SAM	-0.539	7.9	TSI	-8.397	36.3	IOD	-3.151	1.5
IOD	-2.337	5.2	SAM	-1.313	18.0	TSI	-0.034	1.5
TSI	1.844	2.5	IOD	-4.231	2.6	SAM	-0.020	0.2
QBO	0.010	0.2	QBO	0.044	1.2	QBO	-6.823×10 ⁻³	0.1
<i>ii) Global, regional and local factors</i>								
ENSO	7.478	22.6	RH	-0.966	23.1	T	-5.378	24.6
R	0.122	14.6	ENSO	5.135	16.8	ENSO	7.458	19.5
Ws	5.988	10.1	T	-3.542	10.5	RH	-0.276	11.3
SR	0.474	9.4	DFE	1.070×10 ⁻⁵	9.7	DFE	3.886×10 ⁻⁵	10.1
PBL	2.287×10 ⁻³	7.7	PBL	0.043	7.2	PBL	0.070	8.6
T	0.306	7.5	R	0.166	6.5	SR	1.376	8.2
LFE	9.076×10 ⁻⁴	6.8	Wd	-0.087	4.7	R	0.100	4.3
Wd	-0.029	5.1	SR	0.340	4.5	LFE	-5.803×10 ⁻⁴	3.7
RH	-0.257	4.7	IOD	4.900	4.4	Wd	-0.036	3.3
DFE	1.185×10 ⁻⁵	4.2	Ws	-0.601	4.2	Ws	-2.536	2.8
IOD	-12.736	3.7	TSI	-4.195	3.2	IOD	-11.527	1.4
P	6.657×10 ⁻⁴	1.2	LFE	-5.076×10 ⁻³	2.3	P	3.013×10 ⁻⁵	1.0
SAM	-0.339	1.2	P	-1.834×10 ⁻⁴	1.5	TSI	1.670	1.0
TSI	-2.989	0.6	SAM	0.101	0.9	QBO	0.038	0.1
QBO	0.018	0.4	QBO	0.031	0.1	SAM	-0.279	0.1

789

790 The significant contribution of ENSO on variances of the dependent variable (modelled O₃
 791 concentrations) is evident at all three sites, with RIW% indicating ENSO to be the major factor
 792 at AF, and the second most important factor at LT and SK when local, regional and
 793 meteorological factors are included in the model. Therefore, inter-annual variability in O₃
 794 concentrations can most likely be attributed to ENSO cycles. El Niño periods are associated
 795 with drier and warmer conditions in the South African interior, which are conducive to O₃
 796 formation, while cloudy and increased rainfall conditions related to La Niña hinder O₃
 797 production (Balashov et al., 2014). Balashov et al. (2014) indicated that surface O₃
 798 concentrations on the South African Highveld are sensitive to ENSO, with the El Niño period
 799 amplifying O₃ formation. The influence of local and regional meteorological conditions is also

800 indicated by the substantial contributions of R and W_s at AF, as well as T and RH at LT and
801 SK on modelled O₃ levels. At LT, RH made the most substantial contribution to the dependent
802 variable, while T made the most significant contribution to modelled O₃ levels. The negative
803 correlation to T and RH at LT and SK is indicative of higher O₃ concentrations corresponding
804 with drier colder months, as indicated in Fig. 5. Laban et al. (2018) indicated the significance
805 of RH to surface O₃ concentrations in the north-eastern part of South Africa through the
806 statistical analysis of *in situ* O₃ measurements conducted in this region, with RH also negatively
807 correlated to surface O₃ levels. The positive correlation to R and W_s at AF reflects higher O₃
808 concentrations measured during late spring and summer at AF, i.e. October to January, which
809 is a period associated with increased rainfall and less stable meteorological conditions (Fig. 5).
810 The influence of regional open biomass burning during late winter and spring (August to
811 November) on surface O₃ concentrations in this part of South Africa is indicated by the
812 relatively significant contribution of DFE on modelled O₃ concentrations at LT and SK. A
813 recent paper reporting tropospheric O₃ levels measured at four sites in the north-eastern interior
814 of South Africa indicated that O₃ is a regional problem, with O₃ concentration measured at
815 these four sites being similar to levels thereof measured at AF, LT and SK (Laban et al., 2018).
816 A time series of O₃ levels measured from 2010 to 2015 at one of the sites presented by Laban
817 et al. (2018) also indicated higher O₃ concentration corresponding to drier years associated with
818 the ENSO cycle.

819 As indicated in Fig. 8, inter-annual O₃ concentrations at LT decreased from 1995 to 2001,
820 which corresponded to the period when SO₂ and NO₂ concentrations decreased, as discussed
821 in section 3.1. This period of inter-annual decrease in O₃ levels is not reflected in the statistical
822 model. Since LT is a rural background site with low NO_x emissions, it can be considered to be
823 located in a NO_x-limited O₃ production regime where O₃ concentrations correspond with NO_x
824 concentrations, i.e. increase/decrease with increasing/decreasing NO_x. Therefore, the decrease
825 in O₃ concentrations from 1995 to 2001 can be attributed to decreasing NO₂ concentrations
826 during this period, and the factors influencing NO₂ concentrations at LT, i.e. mainly population
827 growth, as discussed above (section 3.2.2).

828 The comparisons between modelled and measured O₃ concentrations (Pane iii in Fig. 11a, b
829 and c) also indicated, as observed for SO₂ and NO₂, that the correlations are significantly
830 improved when local, regional and global factors are included in the model. The R² values,
831 when only global factors are included, i.e. 0.042, 0.048 and 0.094 at AF, LT and SK,
832 respectively, are improved to 0.259, 0.241 and 0.389 at AF, LT and SK, respectively. These

833 correlations can be considered relatively weak, with the exception of a moderate correlation at
834 SK (Sheskin, 2003). These generally weaker correlations can be attributed to the complexity
835 associated with tropospheric O₃ chemistry. Tropospheric O₃ is a secondary atmospheric
836 pollutant with several factors contributing to its variability. In addition, Laban et al. (2018)
837 indicated the significance of the precursor species CO to surface O₃ concentrations in the north-
838 eastern interior of South Africa, which were not measured at any of the sites and included in
839 the model. Swartz et al. (2020) also compared passively derived O₃ concentrations with active
840 O₃ measurements and illustrated limitations associated with the use of passive samplers to
841 determine O₃ concentrations. However, the general trend of measured O₃ concentrations is
842 mimicked by the modelled O₃ values when local, regional and global factors are included in
843 the model, while the overall trend is weakly followed when only global factors are included.
844 Higher and lower O₃ concentrations are underestimated by the MLR model.

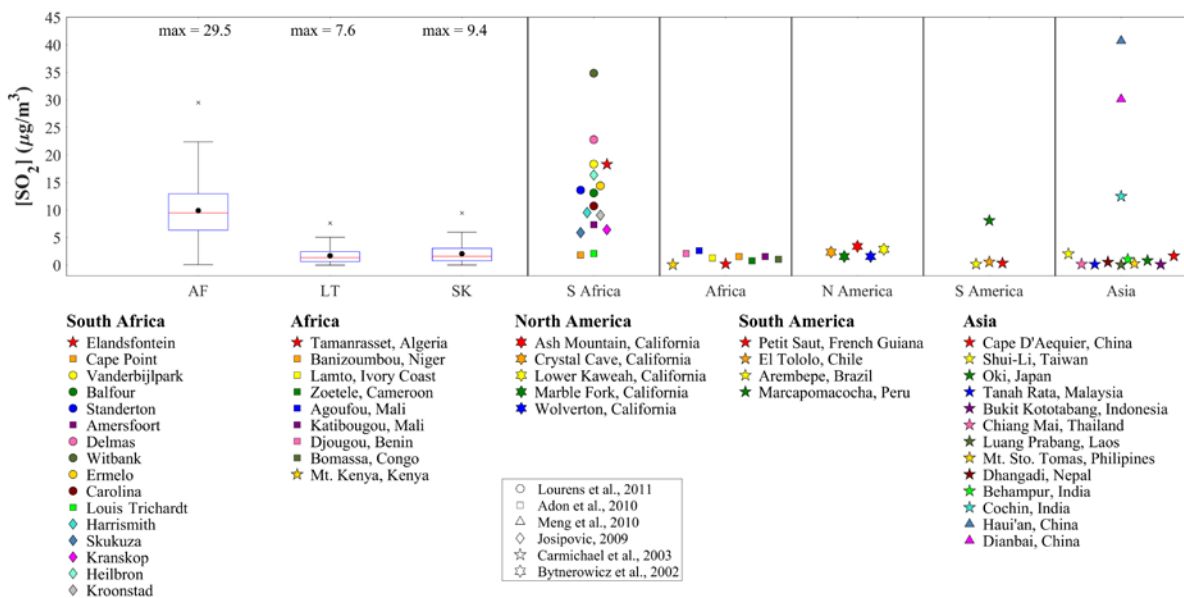
845 The trend lines for the O₃ concentrations measured during the entire sampling periods indicate
846 slight negative slopes at AF and LT (Fig. 11a(iii) and 11b(iii), respectively), and a small
847 positive slope at SK (Fig. 11c(iii)). Annual average decreases in O₃ levels of 0.37 $\mu\text{g}\cdot\text{m}^{-3}\cdot\text{y}^{-1}$
848 and 1.20 $\mu\text{g}\cdot\text{m}^{-3}\cdot\text{y}^{-1}$ were calculated at AF and LT, respectively, while an average annual
849 increase of 0.21 $\mu\text{g}\cdot\text{m}^{-3}\cdot\text{y}^{-1}$ was calculated at SK. However, in general, it seems that O₃
850 concentrations remained relatively constant at all three sites for the entire 19-, 21- and 16-year
851 sampling periods at AF, LT and SK, respectively. Decadal trends of -3.46 (average O₃
852 concentrations from 1997 to 2006 were 52.56 $\mu\text{g}\cdot\text{m}^{-3}$ and average O₃ concentrations from 2007
853 to 2015 were 49.10 $\mu\text{g}\cdot\text{m}^{-3}$) and -9.15 $\mu\text{g}\cdot\text{m}^{-3}\cdot\text{dec}^{-1}$ (average O₃ concentrations from 1995 to
854 2004 were 63.16 $\mu\text{g}\cdot\text{m}^{-3}$ and average O₃ concentrations from 2005 to 2014 were 53.01 $\mu\text{g}\cdot\text{m}^{-3}$)
855 were calculated for AF and LT, respectively, for two decades. Similar to SO₂ and NO₂, the
856 slopes of the linear regression trend lines for the measured and modelled O₃ concentrations
857 when local, regional and global factors are included are exactly the same at AF, LT and SK
858 (Pane iii in Fig. 11a, b and c), which indicates that measured and modelled O₃ trends compares
859 well in spite of low R² values. In addition, relatively good correlations are observed between
860 the slopes of the trend lines of measured O₃ concentrations and modelled O₃ values calculated
861 when only global factors are included at all the sites, signifying the influence of global factors,
862 especially ENSO, as indicated above, on O₃ variability (Pane iii in Fig. 11a, b and c).

863

864 **3.3 Contextualisation**

865 In order to contextualise the long-term SO₂, NO₂ and O₃ concentrations measured with passive
 866 samplers at AF, LT and SK located in the north-eastern interior of South Africa, the statistical
 867 spread of the concentrations of these species determined during the entire sampling period at
 868 each site are compared to average concentrations of these species determined with passive
 869 samplers during other studies in South Africa and Africa, as well as regional sites in other parts
 870 of the world. SO₂, NO₂ and O₃ concentrations determined in this study are related to levels
 871 reported elsewhere in Fig. 12, 13 and 14, respectively.

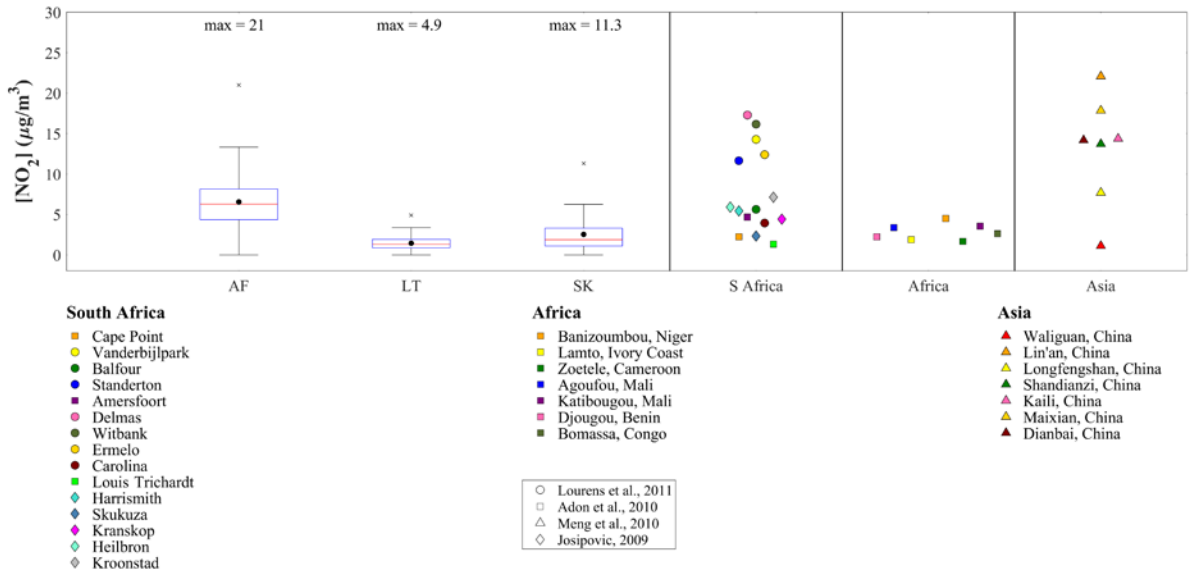
872



873

874 **Figure 12:** Statistical spread of SO₂ concentrations determined during the entire measuring
 875 period at each site compared to mean levels determined with passive samplers
 876 elsewhere. The red line of each box represents the median, the top and bottom
 877 edges of the box the 25th and 75th percentiles, respectively, the whiskers ± 2.7σ
 878 (99.3% coverage if the data has a normal distribution) and the black dots the
 879 average concentrations

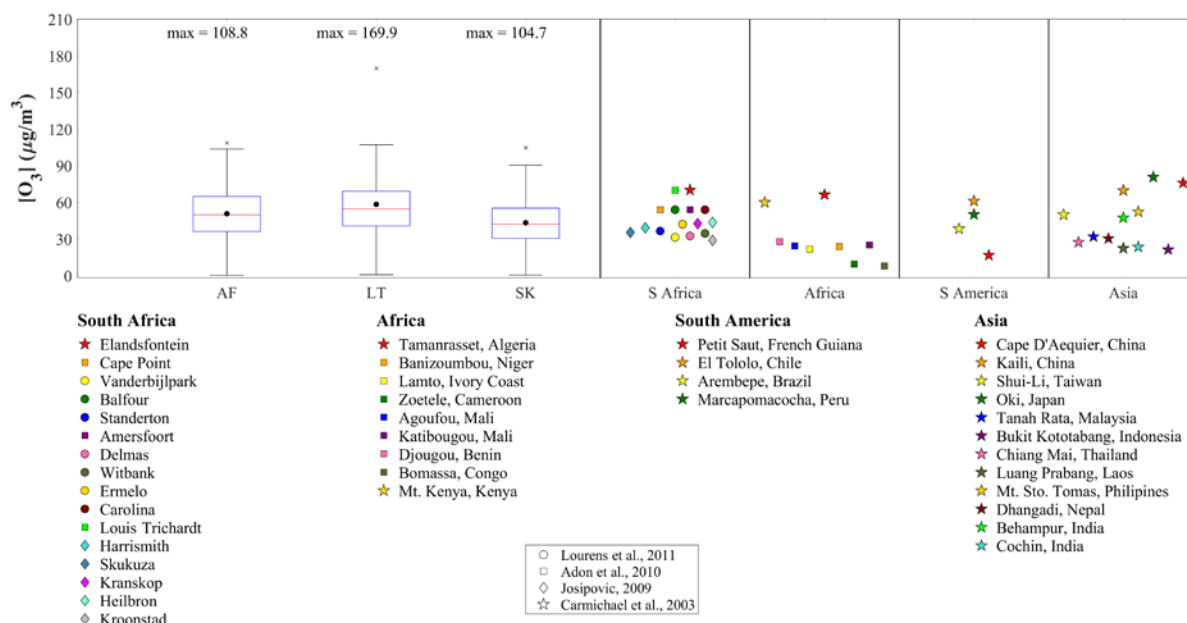
880



881

882 **Figure 13:** Statistical spread of NO_2 concentrations determined during the entire measuring
 883 period at each site compared to mean levels determined with passive samplers
 884 elsewhere. The red line of each box represents the median, the top and bottom
 885 edges of the box the 25th and 75th percentiles, respectively, the whiskers $\pm 2.7\sigma$
 886 (99.3% coverage if the data has a normal distribution) and the black dots the
 887 average concentrations

888



889

890 **Figure 14:** Statistical spread of O_3 concentrations determined during the entire measuring
 891 period at each site compared to mean levels determined with passive samplers
 892 elsewhere. The red line of each box represents the median, the top and bottom
 893 edges of the box the 25th and 75th percentiles, respectively, the whiskers $\pm 2.7\sigma$
 894 (99.3% coverage if the data has a normal distribution) and the black dots the
 895 average concentrations

896

897 As expected, the average and median SO_2 concentrations determined at the industrially
 898 impacted AF ($9.91 \mu g \cdot m^{-3}$ and $9.48 \mu g \cdot m^{-3}$, respectively) site were higher compared to average
 899 and median SO_2 levels determined at the rural background sites LT ($1.70 \mu g \cdot m^{-3}$ and $1.35 \mu g \cdot m^{-3}$,
 900 respectively) and SK ($2.07 \mu g \cdot m^{-3}$ and $1.60 \mu g \cdot m^{-3}$, respectively) for the entire sampling
 901 period at each site. Geospatial maps of SO_2 column amount in the planetary boundary layer
 902 and NO_2 tropospheric column density averaged over the period 2005 to 2015 over southern
 903 Africa (Fig. [A4–A5](#) and [A5–A6](#) respectively) indicate higher average SO_2 and NO_2
 904 concentrations being observed over the region where AF is located. Much lower average SO_2
 905 and NO_2 concentrations are observed over the northernmost parts of the country, where LT is
 906 located, as well as the western region where SK is situated. Therefore, the influence of coal-
 907 fired power stations on SO_2 (and NO_2) levels measured at AF is evident. The average SO_2
 908 levels at AF were similar to average SO_2 concentrations determined at other sites located in the
 909 Mpumalanga Highveld, for which the measurement period was from August 2007 to July 2008
 910 (Lourens et al., 2011). However, the average SO_2 level at AF was significantly lower than the
 911 mean SO_2 levels at Elandsfontein, Delmas and Witbank. Elandsfontein and Delmas are situated

912 within closer proximity to major industrial activities in the Mpumalanga Highveld, while
913 Witbank is a relatively large urban area with numerous large industrial point sources (Lourens
914 et al., 2011). In addition, the average SO₂ concentrations at Vanderbijlpark – an urban area
915 located within the highly industrialised Vaal Triangle region – were also higher compared to
916 levels thereof at AF. Average SO₂ concentrations determined at regional sites in South America
917 and India, i.e. Marcapomacocha and Cochin, respectively, were also similar to mean SO₂ levels
918 determined at AF (Carmichael et al., 2003). The measurement period of the Carmichael et al.
919 (2003) study was 12 months, starting in September 1999 (Carmichael et al., 2003). SO₂
920 concentrations reported for two rural sites in China, i.e. Dianbai and Hai'an were similar to
921 SO₂ levels determined at Witbank (Meng et al., 2010). Meng et al. (2010) presented results
922 obtained during a two-year study that commenced in January 2007. The mean SO₂
923 concentrations determined at LT and SK were similar to average SO₂ concentrations
924 determined at regional background sites in west- and central African sites (Carmichael et al.,
925 2003; Adon et al., 2010), as well as mean SO₂ levels determined at most of the regional sites
926 in North America – measured between May and November 1999, South America and Asia
927 (Bytnerowicz et al., 2002; Carmichael et al., 2003). Adon et al. (2010) presented ambient SO₂,
928 NO₂ and O₃ concentrations measured from 1998 to 2007 at Katibougou in Mali, Banizoumbou
929 in Niger, Lamto in Ivory Coast and Zoetele in Cameroon. The measurement periods for
930 Agoufou in Mali and Djougou in Benin was from 2005 to 2007, while for Bomassa in Congo
931 measurements were reported between 1998 and 2006 (Adon et al., 2010).

932 Similar to SO₂, the mean and median NO₂ levels determined for the respective sampling
933 periods at each site were higher at AF (6.56 µg.m⁻³ and 6.29 µg.m⁻³, respectively) compared to
934 mean and median levels thereof at LT (1.45 µg.m⁻³ and 1.32 µg.m⁻³, respectively) and SK (2.54
935 µg.m⁻³ and 1.89 µg.m⁻³, respectively). Relatively higher NO₂ concentrations were determined
936 at SK compared to LT, which can be attributed to the influence of growing rural communities
937 on the border of the Kruger National Park (Maritz et al., 2020). The mean NO₂ concentrations
938 at AF were lower compared to most of the average NO₂ levels determined at other sites located
939 in the Mpumalanga Highveld within closer proximity to industrial sources, while being similar
940 to mean NO₂ concentrations measured at Balfour and Carolina. In addition, average NO₂ levels
941 at AF were also lower than average NO₂ concentrations determined in the Vaal Triangle
942 (Lourens et al., 2011). Average NO₂ concentrations determined at rural and regional sites in
943 China were higher than mean NO₂ levels at AF, with the exception of Longfengshan that had
944 similar NO₂ concentrations to AF (Meng et al., 2010), which reflects the scale of atmospheric

945 pollution in China. The average NO₂ concentrations at LT and SK were also similar to mean
946 NO₂ levels determined at regional sites in west- and central African sites (Carmichael et al.,
947 2003; Adon et al., 2010), as well as a remote site (Waliguan) in China (Meng et al., 2010).

948 The statistical distribution of O₃ concentrations determined at AF, LT and SK indicates similar
949 surface O₃ levels at all three sites with marginally higher O₃ concentrations determined at LT
950 (58.44 µg.m⁻³ and 54.67 µg.m⁻³, respectively) compared to AF (50.77 µg.m⁻³ and 49.84 µg.m⁻³,
951 respectively) and SK (43.36 µg.m⁻³ and 42.20 µg.m⁻³, respectively). Higher O₃ levels are
952 expected at the rural background LT site due to decreased O₃ titration compared to polluted
953 regions, while LT is also impacted by aged air masses passing over the Mpumalanga Highveld
954 source region as previously indicated. However, the regional O₃ problem in the South Africa
955 interior is reflected by high O₃ concentrations also measured at the industrially influenced AF
956 site, as well as similar O₃ levels determined at other sites in the Mpumalanga Highveld
957 (Lourens et al., 2011). Laban et al. (2018) attributed high regional O₃ concentrations in the
958 north-eastern interior of South Africa to the influence of household combustion and widespread
959 open biomass burning impacting this region. In addition, the influence of rural communities is
960 also reflected by the slightly lower average O₃ levels at SK. O₃ concentrations measured at
961 west- and central Africa sites were lower than South African O₃ levels (Adon et al., 2010), with
962 the exception of Mt Kenya and a site in northern Africa that had similar O₃ concentrations
963 (Carmichael et al., 2003). Similar O₃ concentrations were determined at the South American
964 regional sites, except for Petit Saut that had lower O₃ concentrations (Carmichael et al., 2003).
965 Average O₃ levels determined at some of the regional Asian sites were in the same range as O₃
966 concentrations over the interior of South Africa, while certain sites in Asia had lower mean O₃
967 levels (Carmichael et al., 2003).

968

969 **4. Summary and conclusions**

970 In this study, long-term trends of atmospheric SO₂, NO₂ and O₃ concentrations measured with
971 passive samplers at three sites located in the north-eastern interior of South Africa are
972 presented. This paper illustrates the value of low-cost atmospheric sampling techniques in order
973 to obtain long-term data, especially for regions restricted by logistical accessibility and limited
974 capacity. A 19-year (1997 to 2015), 21-year (1995 to 2015) and 16-year (2000 to 2015) dataset
975 for AF, LT and SK could be evaluated. Long-term temporal trends indicated seasonal and inter-
976 annual variability at all three sites, which could be ascribed to changes in meteorological

977 conditions and/or variances in source contribution. Inter-annual variability indicated periods
978 up until 2003/2004 and 2002 during which SO₂ and NO₂ concentrations, respectively,
979 decreased, followed by periods during which SO₂ and NO₂ levels increased up until 2009 and
980 2007, respectively. These long-term trends were assessed with an MLR model in order to
981 establish the influence of sources, as well as local, regional and global meteorology on
982 atmospheric SO₂, NO₂ and O₃ concentrations.

983 Interdependencies between local, regional and global parameters included in the statistical
984 model indicated the influence of global meteorology on SO₂ variability at all three sites,
985 especially at the rural background site LT. However, population growth was the most
986 substantial factor in the statistical model at the industrially impacted AF site, while the
987 significance of local and regional meteorology was also evident with T being the most
988 significant factor at SK. The important contribution of population growth on modelled SO₂
989 levels at AF was indicative of the impact of increased anthropogenic activities and energy
990 demand in the north-eastern interior of South Africa. Higher SO₂ concentrations associated
991 with lower temperatures reflected the influence of pollution build-up during winter, while the
992 influence of air masses passing over the source region is also evident at SK and LT. Although
993 global parameters contributed to variances in NO₂ concentrations, local and regional factors
994 made more substantial contributions to modelled NO₂ levels. The most significant factor
995 explaining NO₂ variability at all three sites was population growth, while RH was the most
996 important local and regional meteorological factor. Therefore, similar to SO₂, the influence of
997 population growth and associated increases in anthropogenic activities in the north-eastern
998 interior is also reflected in NO₂ levels, while the impacts of increased household combustion
999 associated with growing rural communities are also evident, especially at SK. The negative
1000 correlation to RH indicates higher NO₂ levels associated with drier months, i.e. winter, which
1001 contribute to seasonal variances. ENSO was shown to make a significant contribution to
1002 modelled O₃ levels at all three sites, while the important influence of local and regional
1003 meteorological factors was also evident, especially through significant negative correlations
1004 with T and RH at SK and LT. Inter-annual O₃ variability in this part of South Africa can
1005 therefore most likely be attributed to ENSO cycles, while seasonal patterns are attributed
1006 changes in local and regional meteorology.

1007 The decreases in SO₂ and NO₂ concentrations from 1995 were attributed to the implementation
1008 of mitigation policies by industries post the establishment of the new democracy in South
1009 Africa. However, these improvements were offset from 2002 due to rapid economic growth

1010 associated with increased industrial activities, as well as the increase in population growth
1011 accompanied by higher energy demand. The 19-year trend lines for SO₂ and NO₂ at AF
1012 indicated an increase in SO₂ and NO₂ concentrations over the 19-year sampling period. In
1013 addition, an upwards trend in NO₂ levels was also evident at SK, signifying the influence of
1014 the growing rural communities on the border of the Kruger National Park. Marginal trends
1015 were observed for SO₂ at SK, as well as SO₂ and NO₂ at LT. Trend analysis of O₃ at all three
1016 sites indicated that O₃ concentrations remained relatively constant at all three sites for the entire
1017 19-, 21- and 16-year sampling periods at AF, LT and SK, respectively.

1018 As expected, SO₂ and NO₂ concentrations were higher at AF compared to levels thereof at the
1019 rural background sites LT and SK. SO₂ levels at AF were similar to levels of these species
1020 determined with passive samplers at other sites within the Mpumalanga Highveld with the
1021 exception of sites closer to the major industrial sources. NO₂ levels at AF were generally lower
1022 than NO₂ concentrations determined at sites within the source region, as well as than regional
1023 sites in China. SO₂ and NO₂ concentrations determined at LT and SK were similar to levels
1024 thereof determined with passive samplers at regional and rural sites in Africa and other parts
1025 of the world. The regional problem of O₃ in the interior of South Africa was also evident, with
1026 similar O₃ levels determined at all three sites.

1027

1028 5. Data availability

1029 [The data of this paper are available upon request to Pieter van Zyl \(pieter.vanzyl@nwu.ac.za\)](#)
1030 [or Paul Beukes \(paul.beukes@nwu.ac.za\).](#)

1031

1032 **Acknowledgements**

1033 The authors would like to thank the International Global Atmospheric Chemistry programme
1034 for endorsing the DEBITS programme, as well as Sasol and Eskom for financial support of the
1035 South African INDAAF project. Assistance with sample deployment and collection by Ms
1036 Carin van der Merwe is also acknowledged, as well as the site operators, who include: Memory
1037 Deacon at AF; Chris James at LT; and Navashni Govender, Walter Kubheka, Eva Gardiner
1038 and Joel Tleane at SK.

1039

1040 **References**

- 1041 Adon, M., Galy-Lacaux, C., Delon, C., Yoboue, V., Solmon, F. & Kaptue Tchente, A. T.
1042 2013. Dry deposition of nitrogen compounds (NO₂, HNO₃, NH₃), sulfur dioxide and ozone in
1043 west and central African ecosystems using the inferential method. *Atmospheric Chemistry and*
1044 *Physics*, 13, 11351-11374, doi: 10.5194/acp-13-11351-2013.
- 1045 Adon, M., Galy-Lacaux, C., Yoboué, V., Delon, C., Lacaux, J. P., Castera, P., Gardrat, E.,
1046 Pienaar, J. J., Al Ourabi, H., Laouali, D., Diop, B., Sigha-Nkamdjou, L., Akpo, A., Tathy, J.
1047 P., Lavenu, F. & Mougin, E. 2010. Long term measurements of sulfur dioxide, nitrogen
1048 dioxide, ammonia, nitric acid and ozone in Africa using passive samplers. *Atmospheric*
1049 *Chemistry and Physics*, 10, 7467-7487, doi: 10.5194/acp-10-7467-2010.
- 1050 Balashov, N. V., Thompson, A. M., Piketh, S. J. & Langerman, K. E. 2014. Surface ozone
1051 variability and trends over the South African Highveld from 1990 to 2007. *Journal of*
1052 *Geophysical Research: Atmospheres*, 119, 20, doi: 10.1002/2013JD020555.
- 1053 Bencherif, H., Diab, R. D., Portafaix, T., Morel, B., Keckhut, P. & Moorgawa, A. 2006.
1054 Temperature climatology and trend estimates in the UTLS region as observed over a southern
1055 subtropical site, Durban, South Africa. *Atmospheric Chemistry and Physics*, 6, 5121-5128, doi:
1056 10.5194/acp-6-5121-2006.
- 1057 Booyens, W., Beukes, J.P., Van Zyl, P.G., Ruiz-Jimenez, J., Kopperi, M., Riekkola, M-L.,
1058 Josipovic, M., Vakkari, V., and Laakso, L. 2019. Assessment of polar organic aerosols at a
1059 regional background site in southern Africa. *Journal of Atmospheric Chemistry*, 76, 89–113,
1060 doi:10.1007/s10874-019-09389-y.
- 1061 Bytnerowicz, A., Tausz, M., Alonso, R., Jones, D., Johnson, R. & Grulke, N. 2002. Summer-
1062 time distribution of air pollutants in Sequoia National Park, California. *Environmental*
1063 *Pollution*, 118, 187-203, doi: 10.1016/S0269-7491(01)00312-8.
- 1064 Carmichael, G. R., Ferm, M., Thongboonchoo, N., Woo, J.-H., Chan, L. Y., Murano, K., Viet,
1065 P. H., Mossberg, C., Bala, R., Boonjawat, J., Upatum, P., Mohan, M., Adhikary, S. P., Shrestha,
1066 A. B., Pienaar, J. J., Brunke, E. B., Chen, T., Jie, T., Guoan, D., Peng, L. C., Dhiharto, S.,
1067 Harjanto, H., Jose, A. M., Kimani, W., Kirouane, A., Lacaux, J.-P., Richard, S., Barturen, O.,
1068 Cerda, J. C., Athayde, A., Tavares, T., Cotrina, J. S. & Bilici, E. 2003. Measurements of sulfur
1069 dioxide, ozone and ammonia concentrations in Asia, Africa, and South America using passive
1070 samplers. *Atmospheric Environment*, 37, 1293-1308, doi: 10.1016/S1352-2310(02)01009-9.
- 1071 Connell, D. W. 2005. *Basic concepts of environmental chemistry*, CRC Press.
- 1072 Conradie, E. H., Van Zyl, P. G., Pienaar, J. J., Beukes, J. P., Galy-Lacaux, C., Venter, A. D. &
1073 Mkhathshwa, G. V. 2016. The chemical composition and fluxes of atmospheric wet deposition
1074 at four sites in South Africa. *Atmospheric Environment*, 146, 113-131, doi:
1075 10.1016/j.atmosenv.2016.07.033.
- 1076 Dhammapala, R. S. 1996. *Use of diffusive samplers for the sampling of atmospheric pollutants*.
1077 M.Sc, Potchefstroom University for CHE.
- 1078 Draxler, R. R. & Hess, G. D. 2014. Description of the HYSPLIT_4 modelling system. 7 ed.
1079 Silver Spring, Maryland: Air Resources Laboratory.

- 1080 Ferm, M. 1991. A Sensitive Diffusional Sampler. *IVL Report L91*. Göteborg, Sweden: Swedish
1081 Environmental Research Institute.
- 1082 Fowler, D., Pilegaard, K., Sutton, M. A., Ambus, P., Raivonen, M., Duyzer, J., Simpson, D.,
1083 Fagerli, H., Fuzzi, S., Schjoerring, J. K., Granier, C., Neftel, A., Isaksen, I. S. A., Laj, P.,
1084 Maione, M., Monks, P. S., Burkhardt, J., Daemmgen, U., Neiryneck, J., Personne, E., Wichink-
1085 Kruit, R., Butterbach-Bahl, K., Flechard, C., Tuovinen, J. P., Coyle, M., Gerosa, G., Loubet,
1086 B., Altimir, N., Gruenhage, L., Ammann, C., Cieslik, S., Paoletti, E., Mikkelsen, T. N., Ro-
1087 Poulsen, H., Cellier, P., Cape, J. N., Horváth, L., Loreto, F., Niinemets, Ü., Palmer, P. I., Rinne,
1088 J., Misztal, P., Nemitz, E., Nilsson, D., Pryor, S., Gallagher, M. W., Vesala, T., Skiba, U.,
1089 Brüggemann, N., Zechmeister-Boltenstern, S., Williams, J., O'dowd, C., Facchini, M. C., De
1090 Leeuw, G., Flossman, A., Chaumerliac, N. & Erisman, J. W. 2009. Atmospheric composition
1091 change: Ecosystems–Atmosphere interactions. *Atmospheric Environment*, 43, 5193-5267, doi:
1092 10.1016/j.atmosenv.2009.07.068.
- 1093 Garstang, M., Tyson, P. D., Swap, R., Edwards, M., Källberg, P. & Lindesay, J. A. 1996.
1094 Horizontal and vertical transport of air over southern Africa. *Journal of Geophysical Research*
1095 *Atmospheres*, 101, 16, doi: 10.1029/95JD00844.
- 1096 Gierens, R.T., Henriksson, S., Josipovic, M., Vakkari, V., Van Zyl, P.G., Beukes, J.P., Wood,
1097 C.R., and O'Connor, E.J. 2019. Observing continental boundary-layer structure and evolution
1098 over the South African savannah using a ceilometer. *Theoretical and Applied Climatology*,
1099 136, 333–346, doi:10.1007/s00704-018-2484-7.
- 1100 He, J. & Bala, R. 2008. Draft Report on passive sampler inter-comparison under Malé
1101 declaration. *Malé Declaration on Control and Prevention of Air Pollution and its Likely*
1102 *Transboundary Effect for South Asia*. Singapore: National University of Singapore.
- 1103 Hewitson, B. C. & Crane, R. G. 2006. Consensus between GCM climate change projections
1104 with empirical downscaling: precipitation downscaling over South Africa. *International*
1105 *Journal of Climatology*, 26, 1315-1337, doi: 10.1002/joc.1314.
- 1106 ICDA (International Chromium Development Association) 2012. High carbon charge grade
1107 ferrochromium Statistics. *Statistical Bulletin 2012*. Paris, France: International Chromium
1108 Development Association.
- 1109 ICDA 2013. Statistical Bulletin 2013 (based on 2012 data). International Chromium
1110 Development Association.
- 1111 [International Energy Agency. 2020. Data and statistics \[Online\]. Available:](https://www.iea.org/data-and-statistics/data-tables?country=SOUTHAFRIC)
1112 <https://www.iea.org/data-and-statistics/data-tables?country=SOUTHAFRIC> [Accessed 14
1113 [May 2020](#)]
- 1114 ISO Survey 2015. Available: <http://www.iso.org/iso/iso-survey> [Accessed 23 January 2017].
- 1115 Inglesi-Lotz, R. & Blignaut, J. 2011. Estimating the price elasticity for demand for electricity
1116 by sector in South Africa. *South African Journal of Economic and Management Sciences*, Vol
1117 14, Iss 4, Pp 449-465 (2011), 449, doi: 10.4102/sajems.v14i4.134.
- 1118 Jaars, K., Beukes, J. P., Van Zyl, P. G., Venter, A. D., Josipovic, M., Pienaar, J. J., Vakkari,
1119 V., Aaltonen, H., Laakso, H., Kulmala, M., Tiitta, P., Guenther, A., Hellén, H., Laakso, L. &
1120 Hakola, H. 2014. Ambient aromatic hydrocarbon measurements at Welgegund, South Africa.

- 1121 *Atmospheric Chemistry and Physics Discussions*, 14, 7075-7089, doi: 10.5194/acp-14-7075-
1122 2014.
- 1123 Josipovic, M. 2009. *Acidic deposition emanating from the South African Highveld: A critical*
1124 *levels and critical loads assessment*. PhD, University of Johannesburg.
- 1125 Josipovic, M., Annegarn, H. J., Kneen, M. A., Pienaar, J. J. & Piketh, S. J. 2011. Atmospheric
1126 dry and wet deposition of sulphur and nitrogen species and assessment of critical loads of acidic
1127 deposition exceedance in South Africa. *South African Journal Science*, 107, 10, doi:
1128 10.4102/sajs.v107i3/4.478.
- 1129 Kaufman, Y. J., Ichoku, C., Giglio, L., Korontzi, S., Chu, D. A., Hao, W. M., Li, R. R. &
1130 Justice, C. O. 2003. Fire and smoke observed from the Earth Observing System MODIS
1131 instrument - products, validation, and operational use. *International Journal of Remote*
1132 *Sensing*, 24, 1765-1781, doi: 10.1080/01431160210144741.
- 1133 Kleynhans, E., Beukes, J. P., Van Zyl, P. G., Bunt, J., Nkosi, N. & Venter, M. 2017. The Effect
1134 of Carbonaceous Reductant Selection on Chromite Pre-reduction. *Metallurgical & Materials*
1135 *Transactions B*, 48, 827-840, doi: 10.1007/s11663-016-0878-4.
- 1136 KMNI. 2016a. *monthly DMI HadISST1* [Online]. Available:
1137 [http://climexp.knmi.nl/getindices.cgi?WMO=UKMODData/hadisst1_dmi&STATION=DMI_](http://climexp.knmi.nl/getindices.cgi?WMO=UKMODData/hadisst1_dmi&STATION=DMI_HadISST1&TYPE=i&id=someone@somewhere)
1138 [HadISST1&TYPE=i&id=someone@somewhere](http://climexp.knmi.nl/getindices.cgi?WMO=UKMODData/hadisst1_dmi&STATION=DMI_HadISST1&TYPE=i&id=someone@somewhere) [Accessed 22 December 2016].
- 1139 KMNI. 2016b. *monthly measured total solar irradiance* [Online]. Available:
1140 [http://climexp.knmi.nl/getindices.cgi?WMO=PMODData/tsi&STATION=measured_total_so](http://climexp.knmi.nl/getindices.cgi?WMO=PMODData/tsi&STATION=measured_total_solar_irradiance&TYPE=i&id=someone@somewhere)
1141 [lar_irradiance&TYPE=i&id=someone@somewhere](http://climexp.knmi.nl/getindices.cgi?WMO=PMODData/tsi&STATION=measured_total_solar_irradiance&TYPE=i&id=someone@somewhere) [Accessed 22 December 2016].
- 1142 Korhonen, K., Giannakaki, E., Mielonen, T., Pfüller, A., Laakso, L., Vakkari, V., Baars, H.,
1143 Engelmann, R., Beukes, J. P., Van Zyl, P. G., Ramandh, A., Ntsangwane, L., Josipovic, M.,
1144 Tiitta, P., Fourie, G., Ngwana, I., Chiloane, K. & Komppula, M. 2014. Atmospheric boundary
1145 layer top height in South Africa: measurements with lidar and radiosonde compared to three
1146 atmospheric models. *Atmospheric Chemistry and Physics*, 14, 4263-4278, doi: 10.5194/acp-
1147 14-4263-2014.
- 1148 Kraha, A., Turner, H., Nimon, K., Reichwein Zientek, L. & Henson, R. K. 2012. Tools to
1149 support interpreting multiple regression in the face of multicollinearity. *Frontiers In*
1150 *Psychology*, 3, 1-16, doi: 10.3389/fpsyg.2012.00044.
- 1151 Laakso, L., Vakkari, V., Virkkula, A., Laakso, H., Backman, J., Kulmala, M., Beukes, J. P.,
1152 Van Zyl, P. G., Tütta, P., Josipovic, M., Pienaar, J. J., Chiloane, K., Gilardoni, S., Vignati, E.,
1153 Wiedensohler, A., Tuch, T., Birmili, W., Piketh, S., Collett, K. & Fourie, G. D. 2012. South
1154 African EUCAARI measurements: seasonal variation of trace gases and aerosol optical
1155 properties. *Atmospheric Chemistry & Physics*, 12, 1847-1864, doi: 10.5194/acp-12-1847-2012.
- 1156 Laban, T. L., Van Zyl, P. G., Beukes, J. P., Vakkari, V., Jaars, K., Borduas-Dedekind, N.,
1157 Josipovic, M., Thompson, A. M., Kulmala, M. & Laakso, L. 2018. Seasonal influences on
1158 surface ozone variability in continental South Africa and implications for air quality.
1159 *Atmospheric Chemistry and Physics* 15491-15514, doi: 10.5194/acp-18-15491-2018.

- 1160 Lacaux, J. P., Tathy, J. P. & Sigha, L. 2003. Acid wet deposition in the tropics: Two case
 1161 studies using DEBITS measurements. *IGACtivities Newsletter of the International Global*
 1162 *Atmospheric Chemistry Project*.
- 1163 Lorenzo-Seva, U., Ferrando, P. J. & Chico, E. 2010. Two SPSS programs for interpreting
 1164 multiple regression results. *Behavior Research Methods*, 42, 29-35, doi:
 1165 10.3758/BRM.42.1.29.
- 1166 Lourens, A. S., Beukes, J. P., Van Zyl, P. G., Fourie, G. D., Burger, J. W., Pienaar, J. J., Read,
 1167 C. E. & Jordaan, J. H. 2011. Spatial and temporal assessment of gaseous pollutants in the
 1168 Highveld of South Africa. *South African Journal of Science*, 107, 1-8, doi:
 1169 10.4102/sajs.v107i1/2.269.
- 1170 Maritz, P., Beukes, J.P., Van Zyl, P.G., Liousse, C., Gardrat, E., Ramandh, A. and Mkhathswa,
 1171 G.V. 2020. Temporal and source assessments of organic and elemental carbon at sites in the
 1172 northern South African interior. *Journal of Atmospheric Chemistry*, doi:10.1007/s10874-020-
 1173 09398-2, 2020.
- 1174 Marshall, G. 2018. *An observation-based Southern Hemisphere Annular Mode Index* [Online].
 1175 United Kingdom. Available: <http://www.nerc-bas.ac.uk/icd/gjma/sam.html> [Accessed 28
 1176 August 2018].
- 1177 Martins, J. J., Dhammapala, R. S., Lachmann, G., Galy-Lacaux, C. & Pienaar, J. J. 2007. Long-
 1178 term measurements of sulphur dioxide, nitrogen dioxide, ammonia, nitric acid and ozone in
 1179 southern Africa using passive samplers. *South African Journal of Science*, 103, 336-342.
- 1180 Meng, Z.-Y., Xu, X.-B., Wang, T., Zhang, X.-Y., Yu, X.-L., Wang, S.-F., Lin, W.-L., Chen,
 1181 Y.-Z., Jiang, Y.-A. & An, X.-Q. 2010. Ambient sulfur dioxide, nitrogen dioxide, and ammonia
 1182 at ten background and rural sites in China during 2007–2008. *Atmospheric Environment*, 44,
 1183 2625-2631, doi: 10.1016/j.atmosenv.2010.04.008.
- 1184 Meth, O. 2018. *New satellite data reveals the world's largest air pollution hotspot is*
 1185 *Mpumalanga – South Africa* [Online]. Available:
 1186 [https://www.greenpeace.org/africa/en/issues/inspirethemovement/4202/new-satellite-data-](https://www.greenpeace.org/africa/en/issues/inspirethemovement/4202/new-satellite-data-reveals-the-worlds-largest-air-pollution-hotspot-is-mpumalanga-south-africa/)
 1187 [reveals-the-worlds-largest-air-pollution-hotspot-is-mpumalanga-south-africa/](https://www.greenpeace.org/africa/en/issues/inspirethemovement/4202/new-satellite-data-reveals-the-worlds-largest-air-pollution-hotspot-is-mpumalanga-south-africa/) [Accessed 17
 1188 January 2019].
- 1189 Monks, P. S., Granier, C., Fuzzi, S., Stohl, A., Williams, M. L., Akimoto, H., Amann, M.,
 1190 Baklanov, A., Baltensperger, U., Bey, I., Blake, N., Blake, R. S., Carslaw, K., Cooper, O. R.,
 1191 Dentener, F., Fowler, D., Fragkou, E., Frost, G. J., Generoso, S., Ginoux, P., Grewe, V.,
 1192 Guenther, A., Hansson, H. C., Henne, S., Hjorth, J., Hofzumahaus, A., Huntrieser, H., Isaksen,
 1193 I. S. A., Jenkin, M. E., Kaiser, J., Kanakidou, M., Klimont, Z., Kulmala, M., Laj, P., Lawrence,
 1194 M. G., Lee, J. D., Liousse, C., Maione, M., Mcfiggans, G., Metzger, A., Mieville, A.,
 1195 Moussiopoulos, N., Orlando, J. J., O'dowd, C. D., Palmer, P. I., Parrish, D. D., Petzold, A.,
 1196 Platt, U., Pöschl, U., Prévôt, A. S. H., Reeves, C. E., Reimann, S., Rudich, Y., Sellegri, K.,
 1197 Steinbrecher, R., Simpson, D., Ten Brink, H., Theloke, J., Van Der Werf, G. R., Vautard, R.,
 1198 Vestreng, V., Vlachokostas, C. & Von Glasow, R. 2009. Atmospheric composition change –
 1199 global and regional air quality. *Atmospheric Environment*, 43, 5268-5350, doi:
 1200 10.1016/j.atmosenv.2009.08.021.

- 1201 Mphepya, J. N., Galy-Lacaux, C., Lacaux, J. P., Held, G. & Pienaar, J. J. 2006. Precipitation
1202 Chemistry and Wet Deposition in Kruger National Park, South Africa. *Journal of Atmospheric*
1203 *Chemistry*, 53, 169-183, doi: 10.1007/s10874-005-9005-7.
- 1204 Mphepya, J. N., Pienaar, J. J., Galy-Lacaux, C., Held, G. & Turner, C. R. 2004. Precipitation
1205 Chemistry in Semi-Arid Areas of Southern Africa: A Case Study of a Rural and an Industrial
1206 Site. *Journal of Atmospheric Chemistry*, 47, 24, doi: 10.1023/B:JOCH.0000012240.09119.c4.
- 1207 Nathans, L. L., Oswald, F. L. & Nimon, K. 2012. Interpreting Multiple Linear Regression: A
1208 Guidebook of Variable Importance. *Practical Assessment, Research & Evaluation*, 17, 1-19.
- 1209 NOAA. 2015a. *Climate Indices: Monthly Atmospheric and Ocean Time Series* [Online].
1210 Available: <https://www.esrl.noaa.gov/psd/data/climateindices/list/> [Accessed 22 December
1211 2016].
- 1212 NOAA. 2015b. *Monthly Atmospheric and SST Indices* [Online]. Available:
1213 <http://www.cpc.ncep.noaa.gov/data/indices/> [Accessed 22 December 2016].
- 1214 Rorich, R. P. & Galpin, J. S. 1998. Air quality in the Mpumalanga Highveld region, South
1215 Africa. *South African Journal of Science*, 94, 109.
- 1216 Sheskin, D. J. 2003. *Handbook of Parametric and Nonparametric Statistical Procedures*, Boca
1217 Raton, Chapman and Hall/CRC Press.
- 1218 Swartz, J.-S., Van Zyl, P.G., Beukes, J.P., Labuschagne, C., Brunke, E.-G., Portafaix, T., Galy-
1219 Lacaux, C. and Pienaar, J.J. 2020. Twenty-one years of passive sampling monitoring of SO₂,
1220 NO₂ and O₃ at the Cape Point GAW station, South Africa. *Atmospheric Environment*, 222,
1221 117128; doi:10.1016/j.atmosenv.2019.117128, 2020.
- 1222 Tiitta, P., Vakkari, V., Croteau, P., Beukes, J. P., Zyl, P. G. V., Josipovic, M., Venter, A. D.,
1223 Jaars, K., Pienaar, J. J., Ng, N. L., Canagaratna, M. R., Jayne, J. T., Kerminen, V. M., Kokkola,
1224 H., Kulmala, M., Laaksonen, A., Worsnop, D. R. & Laakso, L. 2014. Chemical composition,
1225 main sources and temporal variability of PM₁ aerosols in southern African grassland.
1226 *Atmospheric Chemistry and Physics*, 14, 1909-1927, doi: 10.5194/acp-14-1909-2014.
- 1227 Tohir, A. M., Portafaix, T., Sivakumar, V., Bencherif, H., Pazmiño, A. & Bègue, N. 2018.
1228 Variability and trend in ozone over the southern tropics and subtropics. *Annales Geophysicae*,
1229 36, 381-404, doi: 10.5194/angeo-36-381-2018.
- 1230 Tyson, P. D., Garstang, M. & Swap, R. 1996. Large-Scale Recirculation of Air over Southern
1231 Africa. *Journal of Applied Meteorology*, 35, 18, doi: 10.1175/1520-
1232 0450(1996)035<2218:LSROAO>2.0.CO;2.
- 1233 Vet, R., Artz, R. S., Carou, S., Shaw, M., Ro, C.-U., Aas, W., Baker, A., Bowersox, V. C.,
1234 Dentener, F., Galy-Lacaux, C., Hou, A., Pienaar, J. J., Gillett, R., Forti, M. C., Gromov, S.,
1235 Hara, H., Khodzher, T., Mahowald, N. M., Nickovic, S., Rao, P. S. P. & Reid, N. W. 2014. A
1236 global assessment of precipitation chemistry and deposition of sulfur, nitrogen, sea salt, base
1237 cations, organic acids, acidity and pH, and phosphorus. *Atmospheric Environment*, 93, 3-100,
1238 doi: 10.1016/j.atmosenv.2013.10.060.

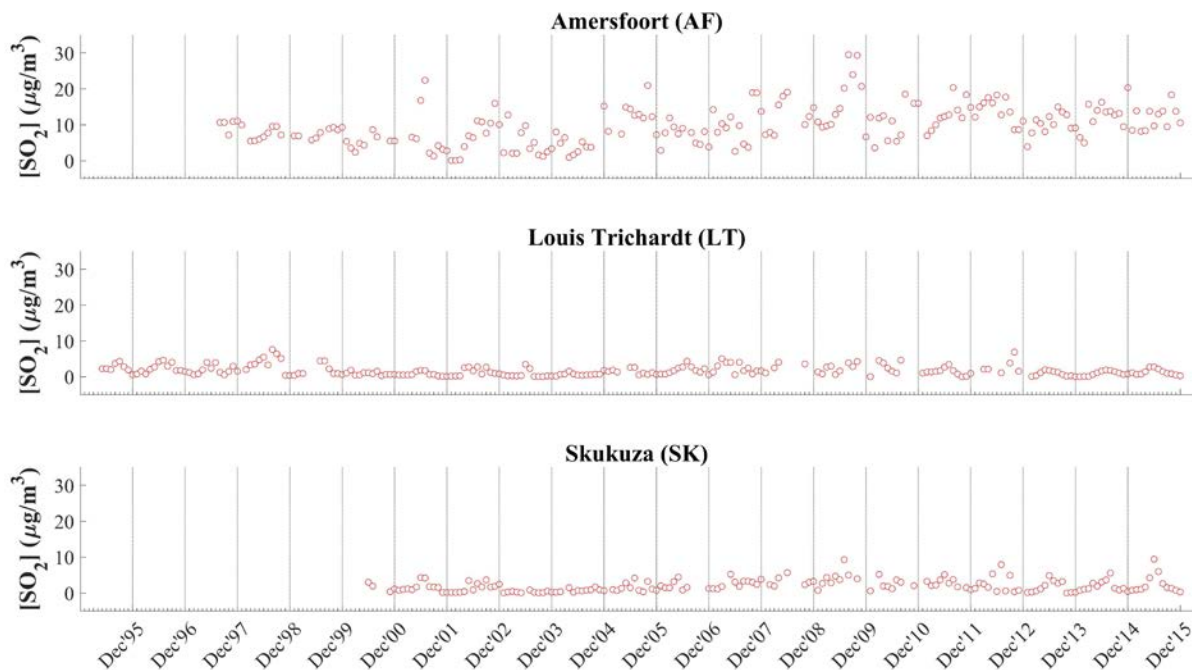
1239 Westcott, G., Tacke, M., Schoeman, N. & Morgan, N. 2007. Impala Platinum Smelter,
1240 Rustenburg: An integrated smelter off-gas treatment solution. *The Journal of the Southern*
1241 *African Institute of Mining and Metallurgy*, 107, 7.

1242 [World Bank. 2019. Data \[Online\]. Available: https://data.worldbank.org/country/south-africa](https://data.worldbank.org/country/south-africa)
1243 [\[Accessed 15 May 2020\].](#)

1244

1245

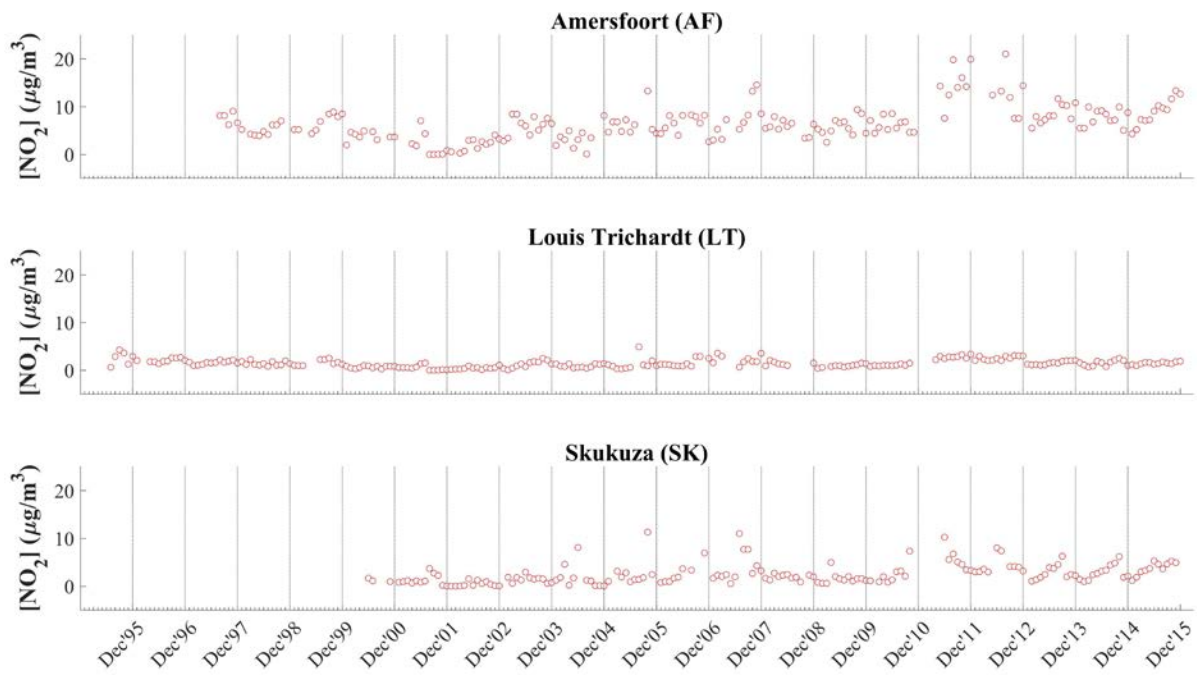
1247



1248

1249 **Figure A1:** Time series of monthly average SO₂ concentrations measured at Amersfoort
1250 (AF), Louis Trichardt (LT) and Skukuza (SK) using passive samplers over the
1251 relevant measurement periods

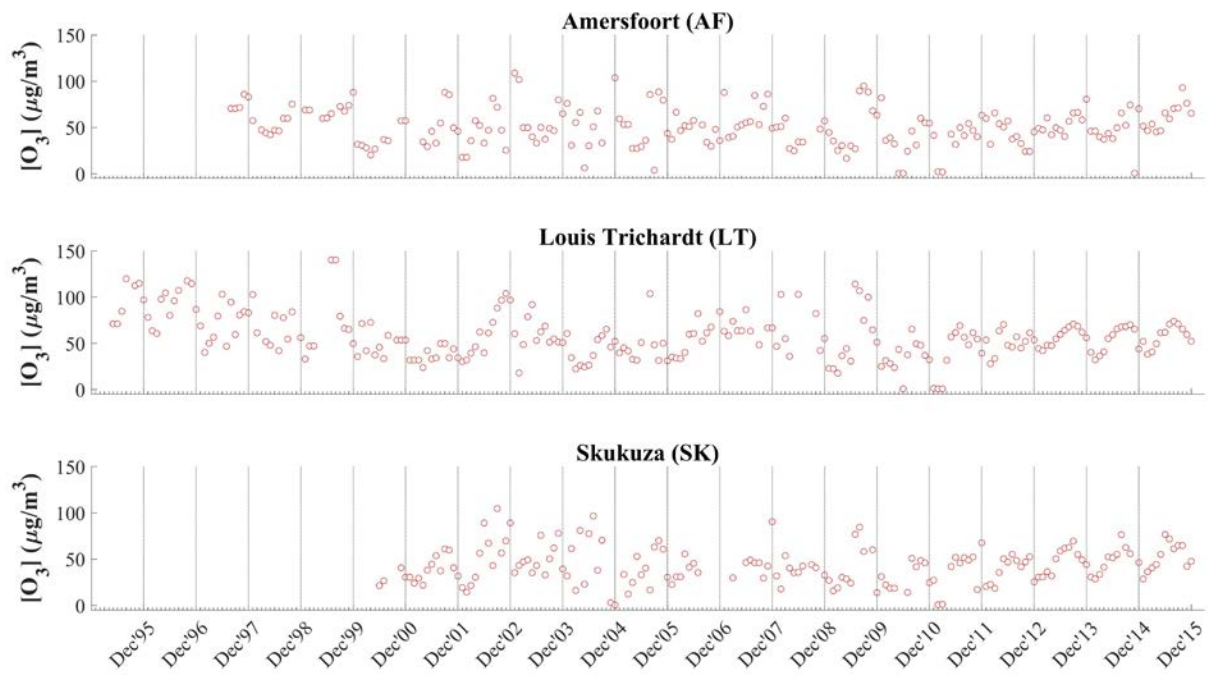
1252



1253

1254 **Figure A2:** Time series of monthly average NO_2 concentrations measured at Amersfoort
 1255 (AF), Louis Trichardt (LT) and Skukuza (SK) using passive samplers over the
 1256 relevant measurement periods

1257



1258

1259 **Figure A3:** Time series of monthly average O₃ concentrations measured at Amersfoort (AF),
 1260 Louis Trichardt (LT) and Skukuza (SK) using passive samplers over the relevant
 1261 measurement periods

1262

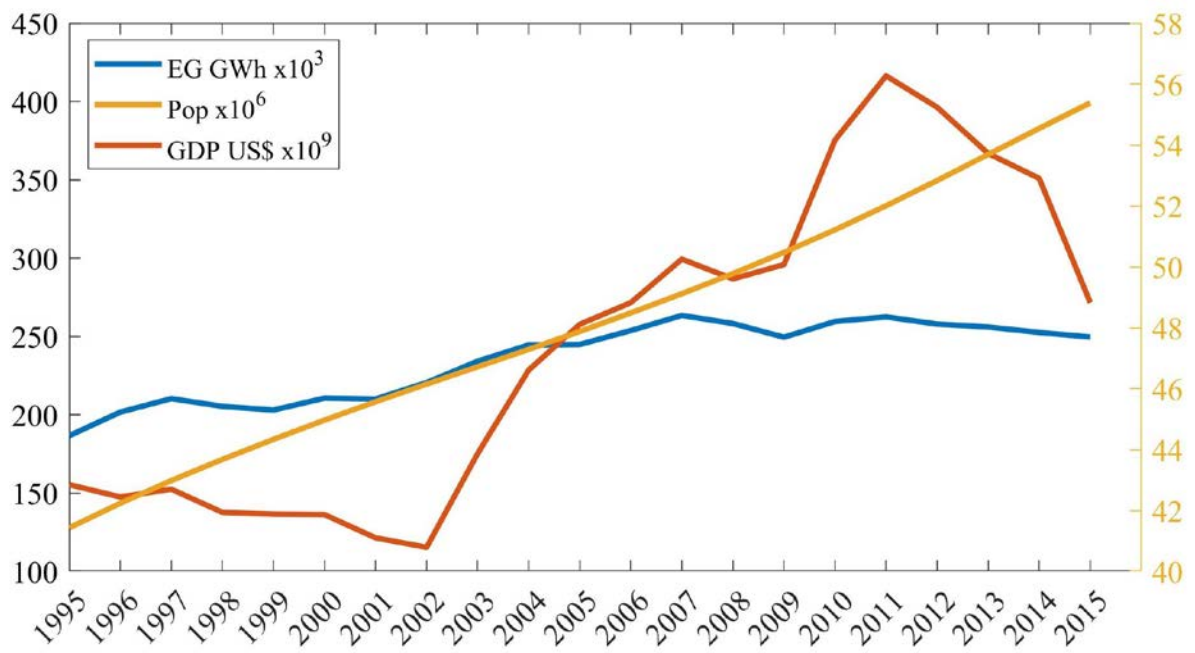


Figure A4: [South African population \(Pop\) and GDP from 1995 to 2015 \(World Bank, 2019\), as well as electricity generation \(EG\) during this period \(International Energy Agency, 2020\)](#)

1263

1264

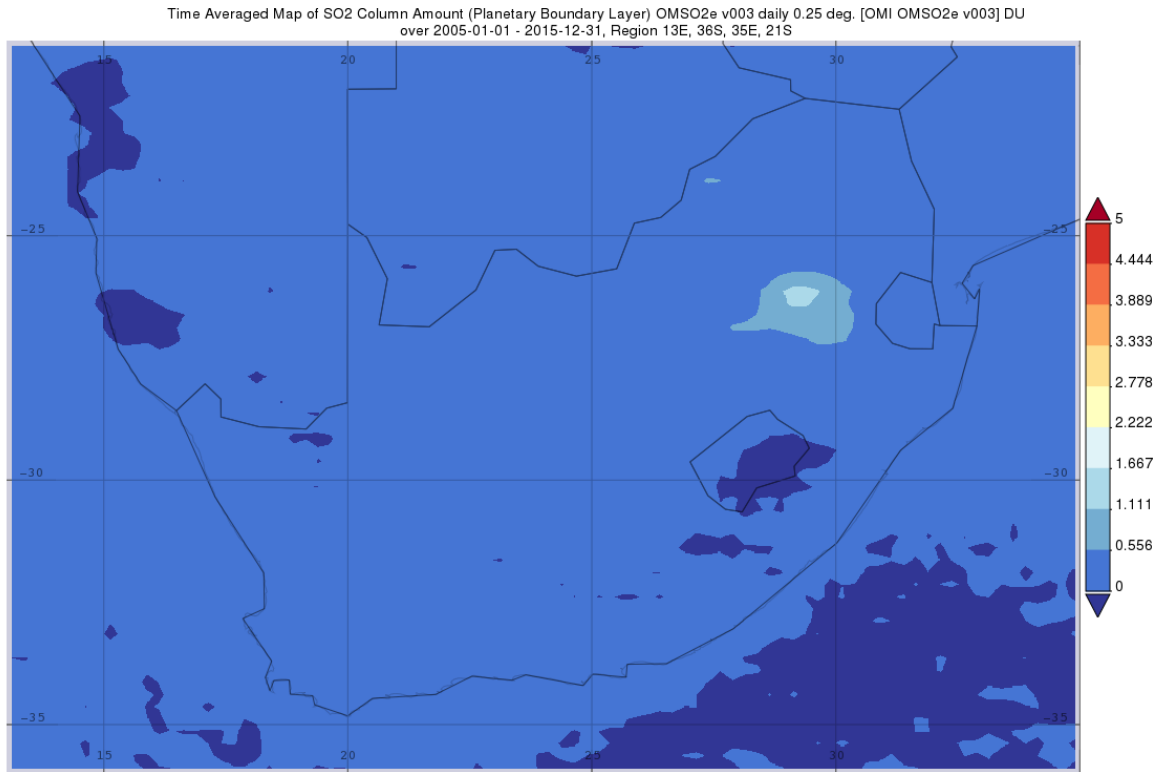
1265

1266

1267

1268

1269



1270

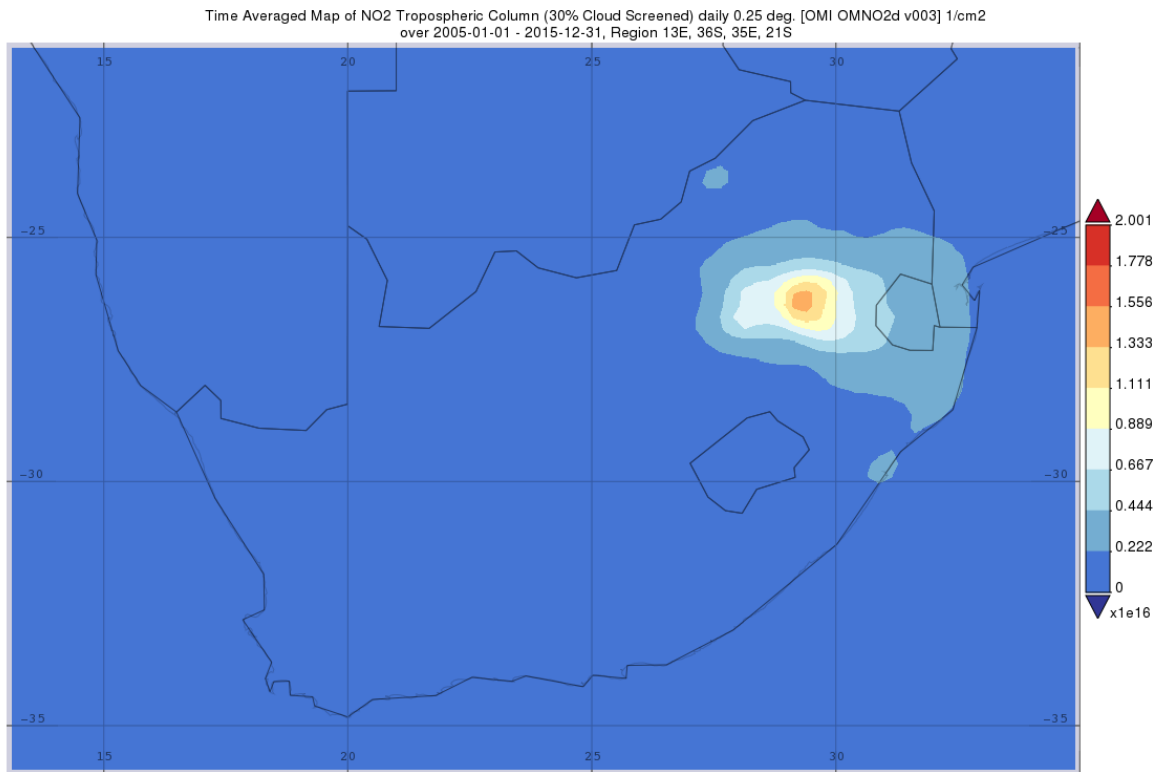
1271

1272

1273

1274

Figure A4A5: Geospatial map of southern Africa depicting the SO₂ column amount averaged over the period 2005 to 2015 obtained using the data from the NASA Giovanni satellite (<https://giovanni.gsfc.nasa.gov/giovanni/>)



1275

1276

1277

1278

Figure A5A6: Geospatial map of southern Africa depicting the NO₂ tropospheric column density averaged over the period 2005 to 2015 obtained using the data from the NASA Giovanni satellite (<https://giovanni.gsfc.nasa.gov/giovanni/>)

1279

1280

1281